TRANSVERSE ISOTROPY:
SOME CONSEQUENCES FOR TRAVEL TIME INVERSION
AND MODELS OF THE OCEANIC CRUST

A THESIS SUBMITTED TO THE GRADUATE DIVISION OF THE
UNIVERSITY OF HAWAII IN PARTIAL FULFILLMENT
OF THE REQUIREMENTS FOR THE DEGREE OF

MASTER OF SCIENCE

IN GEOLOGY AND GEOPHYSICS

DECEMBER 1987

By

Daniel J. Miller

Thesis Committee:

Gerard J. Fryer, Chairman
Eduard Berg
L. Neil Frazer

We certify that we have read this thesis and that, in our opinion, it is satisfactory in scope and quality as a thesis for the degree of Master of Science in Geology and Geophysics.

THESIS COMMITTEE

Gerard J Fryer

Chairman

2 Sept 87

L Neil Frazer

Acknowledgements

Although it says "by Daniel J. Miller" on the title page, the work entailed in producing this thesis was far from a solo effort. Gerard Fryer provided the ideas on which to build and, as I struggled to learn what I needed to know, provided the financial support which allowed me to do so. Gerard's confidence in me, particularly at those numerous times when I really didn't know what I was doing, inspired me to continued effort.

Likewise, Neil Frazer and Ed Berg were always readily available with ideas and advice.

I thank all my friends, particularly my long suffering wife Lynne, for truly being friends and for not only putting up with, but actually assisting, this cranky graduate student during the entire course of this work.

Abstract

Recent evidence for widespread anisotropy demands modification of our models for the oceanic crust. Accommodation of anisotropy in a crustal model requires revision of present seismic interpretation techniques and may result in models which differ dramatically from those obtained assuming isotropy. The consequences of anisotropy for models of the oceanic crust have not been fully explored. In this paper I examine the implications for travel time inversion of the simplest but possibly most widespread form of anisotropy, transverse isotropy with a vertical symmetry axis. Geometrical ray theory provides the framework for this analysis. Numerical computation of travel times for anisotropic models and subsequent travel time inversion demonstrate that layer thicknesses determined for a transversely isotropic structure can be substantially in error if isotropy is assumed, but that the anisotropy *cannot* be identified with travel times from a single refraction branch alone. Complete resolution of transverse isotropy requires narrow to wide angle observations of compressional and shear wave energy; this range of observations is not available from a typical marine seismic survey. When converted shear arrivals are observed, the resulting P and S velocity depth profiles sometimes exhibit characteristics which could arise from an incorrect isotropic parameterization of a transversely isotropic oceanic crust; mismatches in the depth estimates of the two profiles result in apparent abrupt reductions of Poisson's ratio at certain depths.

Table of Contents

List of Tables

List of Figures

I.   Introduction

The assumption of an isotropic oceanic crust has long proven sufficient for the interpretation of marine seismic data. Now, however, increasing evidence suggests that this assumption is invalid. Several workers have identified azimuthal anisotropy in the horizontal plane of the upper oceanic crust (e.g. Stephen, 1985; Shearer and Orcutt, 1986). Anisotropy may also exist in the vertical plane, with a magnitude possibly much greater than the azimuthal anisotropy seen in the horizontal plane.

The seismic velocity in an anisotropic medium depends upon the direction in which it is measured. To understand this behavior we must think in terms of scale. The wavelengths of signals detected in a marine seismic experiment are tens to hundreds of meters long. The waveform seen on a seismograph results from an averaging of the structure sampled in a wavelength. What appears chaotic at a small scale can appear homogeneous at the scale of a wavelength. Structures too small to be resolved in a wavelength, however, still affect the average elastic properties sampled by a seismic disturbance. An aligned sequence of small structures produces a directional variation of the average elastic properties sampled in a wavelength, making the medium effectively anisotropic at a seismic scale. Such aligned structures might be mineral grains (which may themselves be anisotropic), thin layers, fractures, cracks, or pores (Crampin, 1984).

Vertically aligned structures (cracks) cause the azimuthal anisotropy seen in the upper oceanic crust (Stephen, 1985). By contrast, horizontally aligned structures cause anisotropy in the vertical plane. A horizontal fabric imposes hexagonal symmetry with a vertical symmetry axis on the elastic parameters of the medium. In such a system, elastic properties do not vary with azimuth but *do* vary with angle of incidence.

A system with hexagonal symmetry is widely described as being transversely

isotropic. Following Bamford and Crampin (1977), "transverse isotropy" here will refer only to hexagonal symmetry with a *vertical* symmetry axis. The recommendation that transverse isotropy refer only to systems with a vertical symmetry axis has not been universally accepted and Crampin (1987) has suggested the term "azimuthal isotropy" as less ambiguous.

Observations suggest that transverse isotropy is widespread; horizontal fabrics are ubiquitous features of the upper oceanic crust. Sediments are deposited in horizontal beds; laboratory measurements on core samples have established the anisotropy of marine sediments (Bachman, 1979). Likewise, a high concentration of subhorizontal macrocracks observed at DSDP borehole 504B (Newark et al., 1985) point to pronounced anisotropy in the upper crystalline basement (Fryer et al., 1987). Clearly, our isotropic model of the upper oceanic crust requires revision.

Seismic interpretation techniques must be expanded to accommodate anisotropy; failure to do so results in incomplete and inaccurate isotropic models. In this paper I examine the error incurred by an isotropic interpretation of data obtained from an anisotropic structure. I deal with the simplest seismic interpretation technique, travel time inversion for a planar stratified model. I look at the simplest of anisotropic structures, those exhibiting azimuthal isotropy. And I use the simplest possible theory, geometric ray tracing.

A number of workers have addressed the consequences of transverse isotropy for reflection travel times (Levin, 1979; Crampin and Radovich, 1982; Byun, 1984). In this work I investigate the implications of transverse isotropy for refraction travel time analysis. This is done using a combination of ray tracing and travel time inversion for both isotropic and transversely isotropic models. The three major findings are:

- Standard travel time analysis techniques *cannot* identify transverse

2

isotropy in the upper oceanic crust.

- A travel time inversion which accounts for transverse isotropy can yield depth determinations substantially different from those obtained assuming isotropy.

- There *are* observations diagnostic of transverse isotropy, but full resolution of this anisotropy requires modification of experiment design.

II. Anisotropy

Ray Theory

Ray theory is a pragmatic starting point for the study of elastic wave propagation. Conceptually, tracing rays is useful in understanding the seismic behaviour of a model. In forward modeling, ray theory allows the quick calculation of travel times which can be compared to those observed in actual data. Ray theory also provides the means to find a velocity depth profile from the inversion of observed travel times. Travel time inversion is generally the first and often the only step in developing a seismic model from data.

It is instructive to outline geometric ray theory for general anisotropy and then to consider transverse isotropy as a special case. An account of elastic wave propagation in an anisotropic medium requires a complete description of the elastic properties of the medium; this is conveniently done using tensor notation. Strain is expressed in terms of the infinitesimal strain tensor ϵ

$$\epsilon_{kl} = \frac{1}{2}(\frac{\partial \dot{u}_l}{\partial x_k} + \frac{\partial u_k}{\partial x_l})$$

and is related to stress τ by the constitutive relation

$$\tau_{ij} = c_{ijkl}\epsilon_{kl}$$

with summation over repeated subscripts. Newton's second law then provides the momentum equation:

$$\rho\frac{\partial^2 u_i}{\partial t^2} - \frac{\partial}{\partial x_j}(c_{ijkl}\frac{\partial u_k}{\partial x_l}) = f_i. \tag{1}$$

Components of the displacement field $\mathbf{u}$ are functions of both position $\mathbf{x}$ and time t. Density ρ and components c_{ijkl} of the stiffness tensor $\mathbf{c}$ are functions of position $\mathbf{x}$. The stiffness tensor $\mathbf{c}$ is positive definite and its components exhibit the following symmetries (Auld, 1973, vol. 1, pgs. 58 & 148):

$$c_{ijkl} = c_{jikl} = c_{ijlk}$$

4

and

$$c_{ijkl} = c_{klij}.$$

An applied force is specified by components of the source term **f**.

Equation (1) is a hyperbolic differential equation of second order; we seek a solution of (1) which enables us to follow a wavefront W which propagates through the medium.

Consider a wavefront as the leading edge of a disturbance in the displacement field **u** radiating outwards from an impulsive force **f** which occurs in the medium at time $t = 0$. The wavefront expands outward as a closed surface beyond which there is no disturbance in **u**.

Unless the material is ruptured, **u** is continuous across the wavefront, but derivatives of **u** (i.e. $\partial^2 \mathbf{u}/\partial t^2$) experience a jump discontinuity. That the wavefront W is a surface of discontinuity (of the derivatives) of **u** indicates that W is a characteristic surface of equation (1). A characteristic of equation (1) is a closed surface W in space and time defined by $\phi = \phi(\mathbf{x}, t) = 0$. Locally to a point **x** on W, at a scale such that the density and stiffness of the material can be approximated as constants, ϕ is a solution of the " characteristic form":

$$Q(\phi) = \det \left| \frac{c_{ijkl}}{\rho} \frac{\partial \phi}{\partial x_j} \frac{\partial \phi}{\partial x_l} - \left(\frac{\partial \phi}{\partial t} \right)^2 \delta_{ik} \right| = 0 \tag{2}$$

(Courant and Hilbert, 1962, p. 580). When ρ and **c** are functions of position Q will also change with position.

A characteristic surface can be expressed in terms of a one parameter family of surfaces. For a traveling wavefront this parameter is time t. Then ϕ is expressed as

$$\phi(\mathbf{x}, t) = \psi(\mathbf{x}) - t = 0. \tag{3}$$

At some time $t, \psi(\mathbf{x}) = t$ describes the wavefront in space. A vector normal to the wavefront is defined by $\nabla \psi$ where ∇ is the gradient operator in **x** space. The

5

velocity of the wavefront along the trajectory normal to its surface is the normal velocity $\mathbf{v}_n$ found from

$$\mathbf{v}_n = \frac{\nabla\psi}{\nabla\psi \cdot \nabla\psi}. \tag{4}$$

The slowness $\mathbf{p}$ in the medium is defined by $\mathbf{p} = \nabla\psi$. From (4) we have the relations

$$\mathbf{v}_n \cdot \mathbf{p} = 1 \tag{5}$$

and

$$\mathbf{v}_n \cdot \mathbf{v}_n = \frac{1}{\mathbf{p} \cdot \mathbf{p}}.$$

With $\mathbf{p} = \nabla\psi$, $\psi = \mathbf{p} \cdot \mathbf{x}$ and (3) becomes

$$\phi(\mathbf{x}, t) = \mathbf{p} \cdot \mathbf{x} - t = 0. \tag{6}$$

At some time t, $\mathbf{p} \cdot \mathbf{x} = t$ defines a plane in $\mathbf{x}$ space with normal $\mathbf{p}$. The equation $\mathbf{p} \cdot \mathbf{x} - t = 0$ is thus the equation of a plane wave tangent to a point $\mathbf{x}$ on the wavefront W propagating with velocity $\mathbf{v}_n = \mathbf{p}/(\mathbf{p} \cdot \mathbf{p})$ (Figure 1). The wavefront W is enveloped by the plane waves $\mathbf{p} \cdot \mathbf{x} - t = 0$.

Substituting (6) into (2) gives the algebraic equation:

$$Q(p_1, p_2, p_3) = \det \mid \frac{c_{ijkl}}{\rho} p_j p_l - \delta_{ik} \mid = 0. \tag{7}$$

In this form Q defines a three sheeted surface S in slowness space which is referred to as the slowness surface. Equation (7) determines all values of slowness, and hence all plane waves, that exist in a medium for which equation (1) is true.

Substituting the plane wave solution $\mathbf{u} = \mathbf{u}(\mathbf{p} \cdot \mathbf{x} - t)$ into the homogeneous form of (1) with $\mathbf{c}$ and ρ constant yields the eigenvalue equation

$$(\frac{c_{ijkl}}{\rho} p_j p_l - \delta_{ik})u_i = 0 \tag{8}$$

for which a nontrivial solution exists only when the determinant of coefficients is zero, i.e. only when equation (7) is true.

6

By labeling the plane wave propagation speed as $c = (\mathbf{p} \cdot \mathbf{p})^{-1/2}$ the slowness can be written as $\mathbf{p} = c\mathbf{n}$ and the normal velocity is then written as $\mathbf{v}_n = c\mathbf{n}$ where $\mathbf{n}$ is a unit normal to the plane wave. In an anisotropic medium, wave speed c is a function of direction. In terms of wave speed equation (8) is written as

$$\left(\frac{c_{ijkl}}{\rho}n_j n_l - c^2 \delta_{ik}\right)u_i = 0 \tag{9}$$

and (7) becomes

$$Q = \det \mid \frac{c_{ijkl}}{\rho}n_j n_l - c^2 \delta_{ik} \mid = 0. \tag{10}$$

In this form Q defines a normal velocity surface, any point of which gives the velocity of a plane wave in the medium. From equation (5) we see that the normal velocity surface is the polar reciprocal of the slowness surface.

Because the stiffness tensor is real (for the lossless case), positive definite, and symmetric, the matrix $(c_{ijkl}/\rho)n_j n_l$ in equation (9) is Hermitian and its eigenvalues are positive and real with orthogonal eigenvectors. The three eigenvectors give the particle displacement polarizations; the eigenvalues give the square of the propagation speeds for the three types of plane waves.

We can use the plane waves (which envelope the wavefront W) to find a parametric expression for W. To find the surface enveloped by the plane waves we minimize the function $\mathbf{p} \cdot \mathbf{x} - t$ subject to the constraint given by equation (7). Using Lagrange multipliers we have:

$$\nabla_p(\mathbf{p} \cdot \mathbf{x} - t + \lambda Q) = 0$$

where ∇_p is the gradient operator in slowness space and the Lagrange multiplier λ is some constant. This gives for $\mathbf{x}$ on W

$$\mathbf{x} = \lambda \nabla_p Q.$$

As $\nabla_p Q$ is a vector normal to the slowness surface S, we see that the vector $\mathbf{x}$ is perpendicular to S (Kraut, 1963). For the plane wave tangent to W at $\mathbf{x}$, $\mathbf{p} \cdot \mathbf{x} - t = 0$.

7

Substituting $\lambda \nabla_p Q$ for $\mathbf{x}$ in the plane wave equation $\mathbf{p} \cdot \mathbf{x} = t$ gives $\lambda = t/(\mathbf{p} \cdot \nabla_p Q)$, thus a point $\mathbf{x}$ on the wavefront is defined at time t by

$$\mathbf{x} = \frac{t \nabla_p Q}{\mathbf{p} \cdot \nabla_p Q}. \tag{11}$$

The vector $\mathbf{x}$ gives the trajectory of a ray along which energy carried by a disturbance has propagated through the medium. At unit time equation (11) defines a ray velocity surface (Figure 1). Differentiating (11) with respect to time yields a ray velocity $\mathbf{v}_r$ for the medium local to the point $\mathbf{x}$:

$$\mathbf{v}_r = \frac{d\mathbf{x}}{dt} = \frac{\nabla_p Q}{\mathbf{p} \cdot \nabla_p Q}. \tag{12}$$

The wavefront and slowness surface are related in an analogous fashion. Each point $\mathbf{p}$ of the slowness surface defines a tangent plane of the wavefront. Likewise, as $\nabla_p \psi = \mathbf{x}$, each point $\mathbf{x}$ of the wavefront defines a tangent plane of the slowness surface.

We now have all the information needed for tracing rays in an anisotropic medium. The slowness at any point can be obtained from equation (7), the plane wave normal velocity from equation (9), and the ray velocity from equation (12). The ray and plane wave velocities are not necessarily collinear. The direction cosines of the tangent to the ray are $(n_r)_i = (v_r)_i/|\mathbf{v}_r|$ and the direction cosines of the normal to the corresponding plane wave are $(n_n)_i = |\mathbf{v}_n| p_i$. To trace rays across an interface from one medium into another with different elastic properties we need a definition of Snell's law for the anisotropic case.

Snell's Law

For a wavefront incident upon a welded interface between media of different elastic properties, displacement and traction are continuous across the interface.
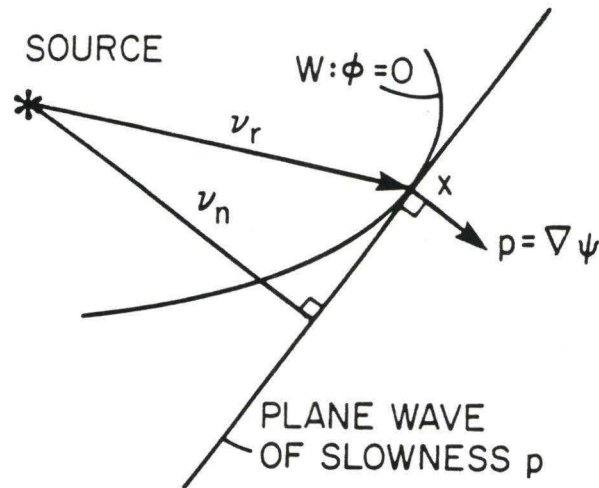
Figure 1: The wavefront W at unit time in an anisotropic medium. At unit time, the vector from the source to a point $\mathbf{x}$ on the wavefront W gives $\mathbf{v}_r$, the ray velocity for point $\mathbf{x}$ on W. The vector extended from the source normal to the plane tangent to W at $\mathbf{x}$ gives $\mathbf{v}_n$, the normal or plane wave velocity. The gradient of W at $\mathbf{x}$ gives the slowness $\mathbf{p}$ of the plane wave. Because W is defined by $\phi(\mathbf{x}, t) = \psi(\mathbf{x}) - t = 0$ (equations (2) and (3)), $\mathbf{p} = \nabla\psi$ and is normal to W at $\mathbf{x}$.

The behavior of the wavefront at the interface can be expressed in terms of the corresponding plane wave. Because displacement and traction are continuous, the component of slowness tangent to the interface in the incident wave is preserved upon reflection or refraction (Auld, 1973, vol. 2, p. 2). Therefore

$$|\mathbf{p}| \sin \theta_n = C \tag{13}$$

where C is a constant and θ_n is the angle of incidence measured between the normal to the plane wave and the normal to the interface. Equation (13) is Snell's law for an interface between two anisotropic media.

III.   Transverse Isotropy

Elastic Parameters

Using abbreviated subscripts, the stiffness matrix for a medium exhibiting transversely isotropic symmetry is

$$\mathbf{C} = \begin{pmatrix} C_{11} & C_{12} & C_{13} & 0 & 0 & 0 \\ C_{12} & C_{11} & C_{13} & 0 & 0 & 0 \\ C_{13} & C_{13} & C_{33} & 0 & 0 & 0 \\ 0 & 0 & 0 & C_{44} & 0 & 0 \\ 0 & 0 & 0 & 0 & C_{44} & 0 \\ 0 & 0 & 0 & 0 & 0 & C_{66} \end{pmatrix} \tag{14}$$

where

$$C_{11} = c_{1111},$$
$$C_{12} = c_{1122} = c_{2211},$$
$$C_{13} = c_{1133} = c_{3311},$$
$$C_{33} = c_{3333},$$
$$C_{44} = c_{2323} = c_{3232},$$
and
$$C_{66} = c_{1212} = c_{2121}.$$

Because $C_{12} = C_{11} - 2C_{66}$, $\mathbf{C}$ in equation (14) contains five independent terms. By virtue of the symmetry of the matrix $\mathbf{C}$, the elastic parameters are invariant under any rotation about the vertical axis.

In an isotropic medium the elastic parameters are invariant under rotation about any axis. For isotropy (14) becomes

$$\mathbf{C} = \begin{pmatrix} C_{11} & C_{13} & C_{13} & 0 & 0 & 0 \\ C_{13} & C_{11} & C_{13} & 0 & 0 & 0 \\ C_{13} & C_{13} & C_{11} & 0 & 0 & 0 \\ 0 & 0 & 0 & C_{44} & 0 & 0 \\ 0 & 0 & 0 & 0 & C_{44} & 0 \\ 0 & 0 & 0 & 0 & 0 & C_{44} \end{pmatrix}$$

with $C_{13} = C_{11} - 2C_{44}$. Here $\mathbf{C}$ has two independent terms, generally expressed using the Lamé parameters λ and μ: $C_{44} = \mu$, $C_{13} = \lambda$, and $C_{11} = \lambda + 2\mu$.

Ray Tracing

Because the elastic parameters in matrix $\mathbf{C}$ in equation (14) are invariant to rotation about the vertical axis, the slowness surface S and the wavefront W for a transversely isotropic medium are axially symmetric. A rotation of the reference frame about the the vertical axis has no effect upon $\mathbf{C}, S,$ or W. In a stratified medium, in which stiffness and density vary only with depth, all waves are confined to propagation in a vertical plane. For ray tracing it is convenient to rotate coordinates so that the x_1 axis is parallel to the horizontal component of the slowness associated with the ray. In the rotated system the horizontal axis is denoted by x, the vertical axis by z (identical to x_3), and the orthogonal direction by y. The p_y component of slowness for the ray will be zero in the rotated reference frame.

To visualize wave propagation in a transversely isotropic medium it is useful to begin the analysis with the homogeneous case for which density and stiffness are constant. Substitution of (14) into (8) gives (with $p_y = 0$ for propagation in the x–z plane):

$$\rho^{-1} \begin{pmatrix} C_{11}p_x^2 + C_{44}p_z^2 & 0 & (C_{13}+C_{44})p_xp_z \\ 0 & C_{66}p_x^2 + C_{44}p_z^2 & 0 \\ (C_{13}+C_{44})p_xp_z & 0 & C_{44}p_x^2 + C_{33}p_z^2 \end{pmatrix} \begin{pmatrix} u_x \\ u_y \\ u_z \end{pmatrix} = \begin{pmatrix} u_x \\ u_y \\ u_z \end{pmatrix}.$$

$$(15)$$

The term in u_y factors out; u_y is the component of displacement perpendicular to the plane of propagation. Thus one eigenvector is completely decoupled from the other two and corresponds to pure mode SH wave motion. The other two eigenvectors have components of displacement confined entirely to the vertical plane. Along a coordinate axis, where p_x or p_z are zero, these eigenvectors correspond to pure mode P and SV wave motion. Along some general direction the displacements are a combination of longitudinal and transverse motion. The waves are referred to as quasi-P (qP) and quasi-SV (qSV). The qP and qSV labels should be used with care as it is possible in some systems for the qP to have purely transverse motion

12

or for the qSV to have purely longitudinal motion in certain directions. The qP, qSV, and SH waves can all travel with different propagation velocities.

In the isotropic case equation (15) becomes

$$\rho^{-1} \begin{pmatrix} C_{11}p_x^2 + C_{44}p_z^2 & 0 & (C_{13}+C_{44})p_xp_z \\ 0 & C_{44}(p_x^2+p_z^2) & 0 \\ (C_{13}+C_{44})p_xp_z & 0 & C_{44}p_x^2 + C_{11}p_z^2 \end{pmatrix} \begin{pmatrix} u_x \\ u_y \\ u_z \end{pmatrix} = \begin{pmatrix} u_x \\ u_y \\ u_z \end{pmatrix}.$$

P, SV, and SH are all pure mode waves, the wave speeds are invariant with direction and both shear waves have equal wave speeds (Auld, 1973, vol 1., pg., 169).

Using (14) in equation (7) with $p_y = 0$ gives $Q(p_x, p_y, p_z) = Q(p, q) = 0$ where the horizontal component of slowness, p_x, is denoted by p and the vertical component, p_z, by q. From the definition of slowness:

$$p = \frac{\sin\theta_n}{c} \quad \text{and} \quad q = \frac{\cos\theta_n}{c} \tag{16}$$

where θ_n is the angle of incidence of the plane wave measured from vertical and c is the plane wave propagation speed. $Q(p, q) = 0$ implies that $q = q(p)$. Equation (7) then gives a cubic in q^2; the six roots are

$$q_P = \pm \left\{ \frac{B - \sqrt{B^2 - 4A_{33}A_{44}C}}{2A_{33}A_{44}} \right\}^{\frac{1}{2}},$$

$$q_{SV} = \pm \left\{ \frac{B + \sqrt{B^2 - 4A_{33}A_{44}C}}{2A_{33}A_{44}} \right\}^{\frac{1}{2}}, \tag{17}$$

and

$$q_{SH} = \pm \left\{ \frac{1 - A_{66}p^2}{A_{44}} \right\}^{\frac{1}{2}}$$

where (following the notation of Červený et al., 1977)

$$A_{11} = C_{11}/\rho, \text{etc.},$$
$$A = A_{13}^2 + 2A_{13}A_{44} - A_{11}A_{33},$$
$$B = A_{33} + A_{44} + Ap^2,$$
$$C = 1 - (A_{11} + A_{44})p^2 + A_{11}A_{44}p^4.$$

13

The positive roots refer to downgoing waves (z is positive down) and the negative roots to upgoing waves. In the isotropic case (17) reduces to

$$q_P = \pm \left\{ \frac{1}{A_{11}} - p^2 \right\}^{\frac{1}{2}}$$

and

$$q_{SV} = q_{SH} = \pm \left\{ \frac{1}{A_{44}} - p^2 \right\}^{\frac{1}{2}}.$$

With these results slowness curves can be constructed in the x–z plane. A rotation of the slowness curve about the z axis will produce the slowness surface in three dimensions. Examples of slowness curves for transversely isotropic media are shown in Figure 2.

Using (14) in equation (7) the components of ray velocity $\mathbf{v}_r$ are determined from equation (12):

$$(v_r)_x = \frac{dx}{dt} = \frac{p(A_{11} + A_{44} - 2A_{11}A_{44}p^2 + Aq^2)}{2 - (A_{11} + A_{44})p^2 - (A_{33} + A_{44})q^2}, \qquad (18)$$

$$(v_r)_z = \frac{dz}{dt} = \frac{q(A_{33} + A_{44} - 2A_{33}A_{44}q^2 + Ap^2)}{2 - (A_{11} + A_{44})p^2 - (A_{33} + A_{44})q^2},$$

for qP and qSV and

$$(v_r)_x = pA_{66},$$

$$(v_r)_z = qA_{44},$$

for SH. For isotropy these reduce to

$$\left. \begin{array}{l} (v_r)_x = pA_{11} \\ (v_r)_z = qA_{11} \end{array} \right\} \text{ for } P \text{ waves and}$$

$$\left. \begin{array}{l} (v_r)_x = pA_{44} \\ (v_r)_z = qA_{44} \end{array} \right\} \text{ for } SV \text{ and } SH \text{ waves.}$$

Ray velocity curves are shown in Figure 2. The ray velocity curve found with equation (12) has a direct relationship with the normal velocity curve determined with equation (10) as shown in Figure 3. Each plane wave which can propagate

14
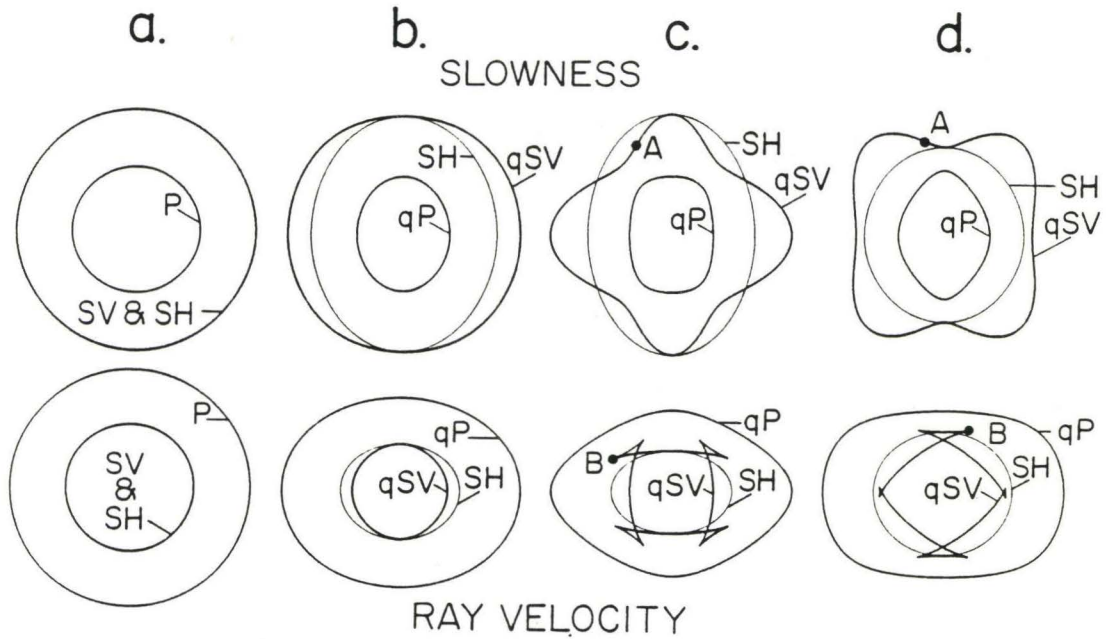
Figure 2: Transversely isotropic slowness curves (upper figures) and corresponding ray velocity curves (lower figures) in the x–z plane. Four examples are shown, including the isotropic case (a). These curves are symmetric about the vertical axis and the horizontal plane. The shape of the curves is determined by the values of the five elastic parameters. Any straight line drawn through the slowness curves can intersect the three sheets in at most six points corresponding to the six roots of equation (7); this implies that the curves are everywhere single valued and that the innermost (the qP) sheet is convex. The qSV slowness curve may have concavities corresponding to triplications in the qSV ray velocity. A point of inflection on the qSV slowness curve (points A in c and d) corresponds to a cusp in the ray velocity curve (points B in c and d). In an isotropic medium, the slowness and ray velocity curves are circular (a).

15

in the medium is tangent to a point on the wavefront. At unit time the wavefront defines a ray velocity surface. Two plane waves with slightly differing slownesses $\mathbf{p}_1$ and $\mathbf{p}_2$ are shown. As $\mathbf{p}_1 \to \mathbf{p}_2$ these intersect at a point on the ray velocity surface. From Figure 3,

$$\theta_r = \theta_n + \arctan \frac{(dc/d\theta_n)}{c} \tag{19}$$

where c is the plane wave propagation speed, θ_r is the angle of incidence of the ray, and θ_n is the angle of incidence of the plane wave.

Snell's Law

For a horizontal interface equation (13) implies that $p = C$, a constant. Snell's law is easy to visualize using slowness curves for the two media as shown in Figure 4. The intersection of the vertical line $p =$ constant with the two slowness surfaces defines the slowness of both the incident and the transmitted wave. Plane wave propagation is in the direction of the slowness vector; the ray direction is normal to the slowness surface. In the isotropic case the direction of plane wave propagation and energy (ray) propagation are parallel.
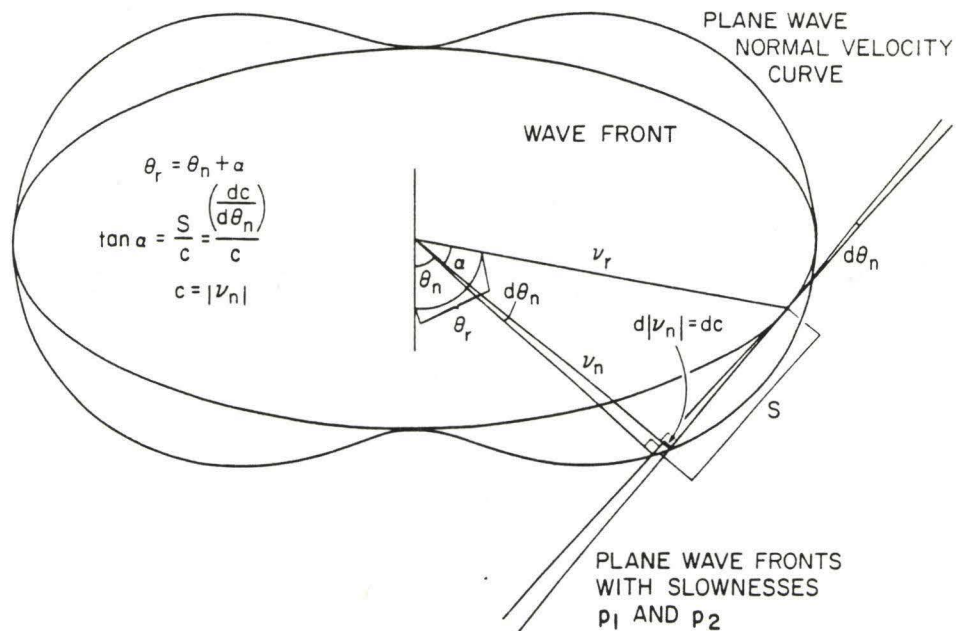
Figure 3: The qP wavefront and the corresponding plane wave normal velocity curve. At unit time, the wavefront defines the ray velocity surface. Plane waves of slownesses $\mathbf{p}_1$ and $\mathbf{p}_2$ are tangent to the wavefront on either side of the point with ray velocity $\mathbf{v}_r$. These plane waves travel with wave speeds differing by $d|\mathbf{v}_n| = dc$ and incident angles differing by $d\theta_n$. As $\mathbf{p}_1 \longrightarrow \mathbf{p}_2$ the plane waves become tangent to the point $\mathbf{v}_r$ on the wavefront. If α is the difference between the plane wave and the ray velocity directions, then $\cos\alpha = |\mathbf{v}_n|/|\mathbf{v}_r| = c/|\mathbf{v}_r|$ and $\sin\alpha = S/|\mathbf{v}_r|$, where the distance S is also given as $S = dc/d\theta_n$, giving the result $\alpha = \tan^{-1}((dc/d\theta_n)/c)$.

17
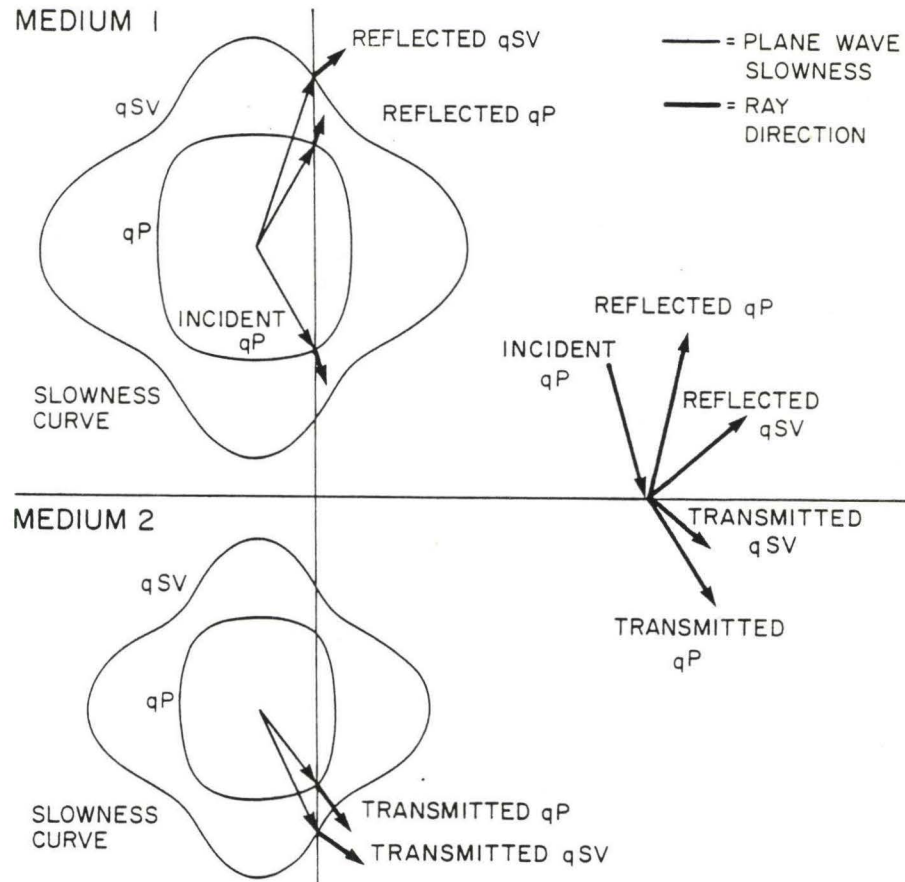
Figure 4: A graphic representation of Snell's law for transverse isotropy. The qP and qSV slowness curves for two media of differing elastic properties are shown on the left and the ray directions, as determined from the slowness curves, are shown on the right. A qP wave in medium 1 incident on a boundary between the two media has the slowness indicated in the slowness curve for medium 1. The ray direction for this wave is normal to the qP slowness surface as shown by the heavy line. From equation (13), for a horizontal interface the horizontal component of slowness p, shown by the vertical line, is preserved in the reflected and transmitted waves. The slowness, and hence ray direction, of the reflected and transmitted waves is determined by the intersection of the vertical line $p = $ constant with the slowness curves. In each case, the corresponding ray, shown by the heavy line, is normal to the slowness surface.

IV.   Travel Time Curves

For a horizontally stratified medium the elastic parameters A_{11}, A_{13}, A_{33}, A_{44}, and A_{66}, are functions of depth z only. For any ray, the horizontal component of slowness p is constant and the vertical component q is a function of z. To find the range x and the travel time t requires an integration over depth. Using (18) gives for qP and qSV

$$x = \int_{z_1}^{z_2} (\frac{dx}{dt})(\frac{dz}{dt})^{-1} dz = p \int_{z_1}^{z_2} \frac{(A_{11} + A_{44} - 2A_{11}A_{44}p^2 + Aq^2)}{q(A_{33} + A_{44} - 2A_{33}A_{44}q^2 + Ap^2)} dz$$

and

$$t = \int_{z_1}^{z_2} (\frac{dz}{dt})^{-1} dz = \int_{z_1}^{z_2} \frac{2 - (A_{11} + A_{44})p^2 - (A_{33} + A_{44})q^2}{q(A_{33} + A_{44} - 2A_{33}A_{44}q^2 + Ap^2)} dz,$$

and for SH

$$x = p \int_{z_1}^{z_2} \frac{A_{66}}{qA_{44}} dz$$

and

$$t = \int_{z_1}^{z_2} \frac{dz}{qA_{44}}$$

for one–way propagation from depth z_1 to z_2.

At the turning point of the ray $q = 0$. This introduces a singularity into the integrands above which may be removed by integrating over q. A bit of algebra reveals for qP and qSV,

$$x = 2p \int_0^{q_1} \frac{A_{11} + A_{44} - 2A_{11}A_{44}p^2 + Aq^2}{D} dq$$

and

$$t = 2 \int_0^{q_1} \frac{2 - (A_{11} + A_{44})p^2 - (A_{33} + A_{44})q^2}{D} dq$$

where

$$
\begin{aligned}
D = {} & A_{11}'p^2(1 - A_{33}p^2 - A_{44}q^2) + A_{33}'q^2(1 - A_{11}p^2 - A_{44}q^2) \\
& + A_{44}'(p^2 + q^2 + 2A_{13}p^2q^2 - A_{33}q^4 - A_{11}p^4) \\
& + 2A_{13}'p^2q^2(A_{13} + A_{44}),
\end{aligned}
$$

19

and for SH

$$x = 2p \int_0^{q_1} \frac{A_{66}}{A'_{66}p^2 + A'_{44}q^2} dq$$

and

$$t = 2 \int_0^{q_1} \frac{dq}{A'_{66}p^2 + A'_{44}q^2}$$

where the prime indicates d/dz.

To visualize the travel path of a wave it is useful to think in terms of homogeneous layers in which rays are straight lines. Figure 5a shows the wavefront from a source at the top of a layer. A ray has been drawn from the source to the point of intersection of the wavefront with the lower interface. The plane wave corresponding to this ray, which is tangent to the wavefront at the point of intersection with the lower boundary, is also drawn. In an anisotropic layer the ray is not necessarily normal to the plane wave front; the direction of energy propagation (the ray) is not the same as the direction of plane wave propagation. In an isotropic layer the wave surface is spherical and the rays are always normal to the plane wave front.

As the wavefront propagates through the layer, each point on the wavefront for which $(v_r)_z > 0$ will eventually intersect the lower boundary once. Receivers placed along the lower boundary will each sample a unique point of the propagating wavefront as shown in Figure 5b. The travel time for the wavefront to reach a receiver can be obtained from the equation for the tangent plane wave, $\mathbf{x} \cdot \mathbf{p} = t$. In Figure 5b, the travel time to receiver E is $t_E = \mathbf{x}_E \cdot \mathbf{p}_E = x_E p_E + z q_E$.

Expressing the travel time as $t = xp + zq$ is equivalent to dividing t into horizontal and vertical components. The time taken for the plane wave to travel a distance x horizontally is xp(Figure 6a); the time taken for the plane wave to travel a distance z vertically is zq (Figure 6b).

For multiple layers t is the sum of the travel time in each layer. For n layers;

$$t = \sum_i^n t_i = \sum_i^n (x_i p_i + z_i q_i) = xp + \sum_i^n z_i q_i.$$

20

a.

SOURCE

θ_n θ_r

WAVE FRONT

PLANE WAVE

RAY

PLANE WAVE
PROPAGATION

APPARENT VELOCITY

$$\frac{|\nu_n|}{\sin\theta_n} = \frac{c}{\sin\theta_n}$$

b.

x_E

WAVE FRONT

Z

RECEIVER

A B C D E F G

c.

TIME t_E

$$\text{TANGENT} = \frac{dt}{dx}\Big|_{x_E} = \frac{\sin\theta_n}{c} = p_E$$

x_E

HORIZONTAL RANGE
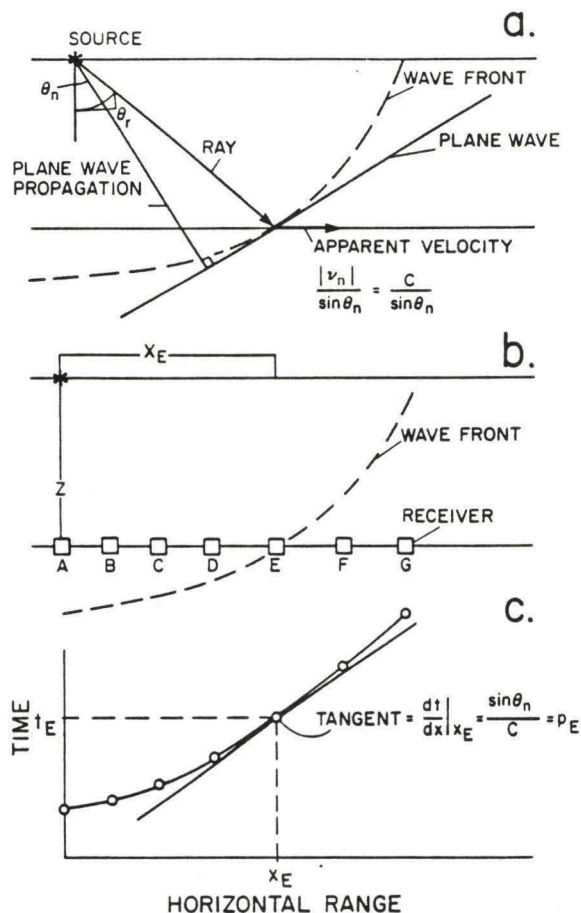
Figure 5: The qP wavefront in a homogenous layer and the corresponding travel time curve. Figure 5a shows the ray incident upon the lower boundary after some time t. This ray has incident angle θ_r. The plane wave for this ray is tangent to the wavefront at the lower boundary of the layer and has incident angle θ_n. The apparent velocity of the point of intersection of the wavefront along the lower boundary is $c/\sin\theta_n$ where c is the plane wave speed. Figure 5b shows a set of receivers placed along the the lower boundary of the layer. Each receiver samples a unique point of the wavefront. The travel time to receiver E is $t_E = x_E p_E + z q_E$ where p_E and q_E are the horizontal and vertical components of slowness of the wavefront incident at receiver E. Plotting the travel time to each receiver as a function of horizontal range gives a travel time curve as shown in Figure 5c. The tangent to the curve at any point gives p, the horizontal component of slowness of the wavefront incident at that range. The tangent at range x_E gives p_E, which is the inverse of the apparent velocity of the wavefront along the interface at range x_E.

21
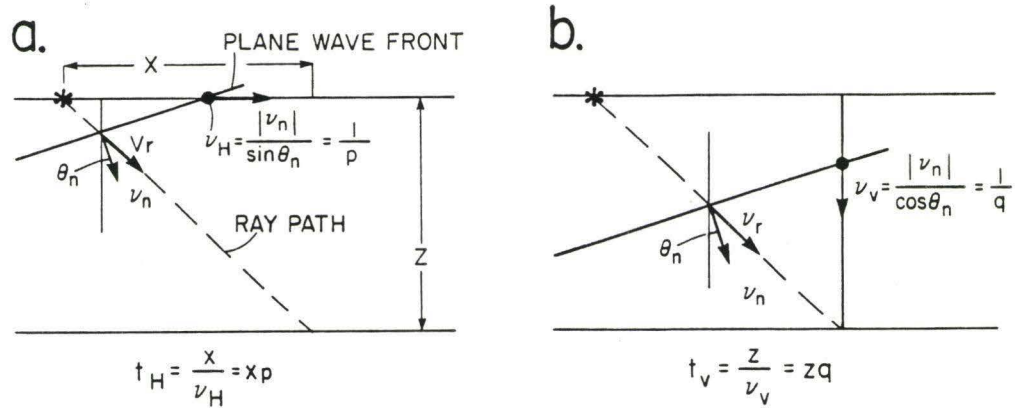
Figure 6: A sketch of horizontal (Figure 6a) and vertical (Figure 6b) components of ray propagation. The ray travels with velocity $\mathbf{v}_r$, the corresponding plane wave with velocity $\mathbf{v}_n$. The apparent velocity of the point of intersection of the plane wave along a horizontal line (Figure 6a) is $v_H = |\mathbf{v}_n|/\sin\theta_n = 1/p$. The horizontal component of travel time for the ray traveling a range x is $t_H = x/v_H = xp$. The apparent velocity of the point of intersection of the plane wave along a vertical line is $v_V = |\mathbf{v}_n|/\cos\theta_n = 1/q$. Thus, the vertical component of travel time for the ray through a layer of thickness z is $t_V = z/v_V = zq$. The total travel time for the ray in the layer is $t = t_H + t_V = xp + zq$.

For a ray reflected at the bottom of a transversely isotropic layer the travel time and range for the upgoing ray are the same as for the downgoing ray. The travel time for any source–receiver geometry can be decomposed into a sum of horizontal components and upgoing and downgoing vertical components:

$$t = \underbrace{xp}_{\text{Horizontal}} + \underbrace{\sum_i z_i q_i}_{\text{Downgoing}} + \underbrace{\sum_j z_j q_j}_{\text{Upgoing}}.$$

Any vertical heterogeneity can be constructed with a series of homogeneous layers. The travel time for a ray traversing a vertical velocity gradient can be determined by taking the limit as the layer thicknesses go to zero.

Plotting travel time to receivers as a function of horizontal distance from the source gives a travel time curve (Figure 5c). Each incidence of the wavefront at a receiver produces one point on the travel time curve. With an infinity of receivers a continuous curve can be constructed; in practice we interpolate between points. For any point on the curve $t(x)$, $t = xp + \sum zq$. Then $dt(x) = pdx + xdp + \sum zdq$. From equation (19) and Figure 3, $\tan \theta_r = x/z = -dq/dp$. This gives the familiar result $dt(x)/dx = p$. From (16) $p = \sin \theta_n/c$. In a stratified medium p is called the ray parameter.

23

V.   Inversion of Travel Time Curves

From a seismic data set we obtain a set of (x, t) observations for the arrival of a particular phase at a set of receivers. Estimates of p are determined from the slope of the travel time curve fit to the (x, t) points. Along a ray

$$dx = dz \tan \theta_r \quad \text{and} \quad dt = v_r dz \sec \theta_r. \tag{20}$$

In an isotropic medium $v_r = v_n$ and $\theta_r = \theta_n$ so that

$$dx = \frac{pv}{(1 - v^2 p^2)^{\frac{1}{2}}} dz \quad \text{and} \quad dt = \frac{dz}{v(1 - v^2 p^2)^{\frac{1}{2}}}$$

where $v = v_r = v_n = v(z)$. For transverse isotropy this is no longer true, but the (x, t, p) values can still be used with these equations to find an isotropic velocity depth function $v(z)$ consistent with the observations.

We can treat each refracted arrival as a ray critically reflected at the top of a layer with horizontal velocity $(v_r)_H = 1/p$. For isotropic layers we can use the plane wave equation $\mathbf{x} \cdot \mathbf{p} - t = 0$ to solve for the layer thicknesses. If v is known for the surface layer (layer 1), then

$$z_1 = \frac{(t_1 - x_1 p_1)}{2q_1} = \frac{\tau_1}{2q_1}$$

where

$$\tau_1 = (t_1 - x_1 p_1),$$

$$q_1 = \left(\frac{1}{v_1^2} - p_1^2\right)^{\frac{1}{2}} = (p_0^2 - p_1^2)^{\frac{1}{2}},$$

p_1 and q_1 are the horizontal and vertical slownesses of the ray critically reflected at the top of layer 2 (bottom of layer 1), $p_0 = 1/v_1$, v_1 is the velocity in layer 1, t_1 is the two way travel time for the critically reflected ray in layer 1, and z_1 is the thickness of layer 1. The value of p_1 is determined from the slope of the travel time

24

curve at the point (x_1, t_1). Then for layer 2, $v_2 = 1/p_1$ and

$$z_2 = \frac{\tau_2 - z_1(p_0^2 - p_1^2)^{\frac{1}{2}}}{(p_1^2 - p_2^2)^{\frac{1}{2}}}.$$

Likewise for layer n,

$$z_n = \frac{\tau_n - \sum_{k=1}^{n-1} z_n(p_{k-1}^2 - p_n^2)^{\frac{1}{2}}}{(p_{n-1}^2 - p_n^2)^{\frac{1}{2}}} \qquad (21)$$

(Diebold and Stoffa, 1981). Thus, with a set of (x, t) observations and corresponding estimates of p, equation (21) provides a set of layer thickness with which to construct a step function $v(z)$. This method of inverting a set of travel time and range observations to a velocity depth function will be referred to as a tau–sum inversion. If $v(z)$ is a smooth function of z this method will distort the true depths; this distortion is compensated for by dense data coverage.

If a layer is transversely isotropic, $1/(v_r) = p$ only when the ray is horizontal and (21) is no longer true. The set of (x, t, p) values can still be used in (21), however, to find a set of apparently legitimate z_n values.

A vertical isotropic velocity gradient dv/dz is found explicitly from equations (20) by assuming that $dv/dz = $ constant and $dv = (dv/dz)dz$ (Dorman and Jacobson, 1981). For transverse isotropy $dv_r = (\partial v_r/\partial z)dz + (\partial v_r/\partial \theta)d\theta$. The function $v(z)$ found by ignoring terms in θ will incorrectly describe the velocity in a transversely isotropic medium.

For a transversely isotropic stratified structure a standard travel time inversion will produce an isotropic velocity depth estimate with no indication that anything is amiss. This estimate can be very misleading; the error will remain undetected until some other method of determining $v(z)$ (such as drilling) reveals inconsistent results. Determination of a gradient structure from turning rays will incur an error dependent upon the particular form of $v_r(z, \theta)$. A comparison of isotropic and transversely isotropic models obtained from synthetic data will be instructive in determining what this error may be.

25

In marine seismic experiments an explosive source over a stratified crust will not excite SH particle motion. Therefore the following discussion involves primarily the qP and qSV modes. The same techniques can be expanded to include SH analysis.

VI. Seismic Models:
Parameterization and Constraints

As shown in section III, the seismic velocities in a transversely isotropic solid are functions of the five independent elastic parameters which define the stiffness matrix of the material. A transversely isotropic seismic model can be specified in terms of these elastic parameters. In a stratified model each parameter is a function of depth only; the seismic velocities are determined as functions of depth and direction (or equivalently, ray parameter) with equation (18) in section III. A model for qP and qSV wave propagation must specify A_{11}, A_{13}, A_{33},and A_{44} as functions of depth (where $A_{11} = C_{11}/\rho$, etc.); a model for SH wave propagation must specify A_{44} and A_{66} as functions of depth. We must now look to theory and experiment to determine appropriate values for these parameters.

Because the stiffness matrix is positive definite (Auld, 1973, vol. 1, pg. 148), certain *a priori* constraints are imposed upon the model parameters:

$$A_{11} \geq A_{66} \geq 0,$$

$$A_{33} \geq 0, \quad A_{44} \geq 0, \tag{22}$$

$$A_{13}^2 \leq A_{33}(A_{11} - A_{66}).$$

Another primary constraint on the model parameters is that the predicted travel times match those observed in seismic data. With discrete noisy data, however, even an isotropic model, for which we seek a profile of only one parameter at a time, is notoriously indeterminate. Quadrupling the number of parameters only exacerbates this problem. For transverse isotropy, the observations made in a standard seismic survey are inherently inadequate to detect the anisotropy. As shown in section IV, an isotropic model can always be found to fit a refraction branch from a transversely isotropic structure. Placing uncertainties in the data aside, we must first determine

27

what observations are required both to detect the anisotropy and to resolve the elastic parameters of a transversely isotropic structure.

Travel times observed in seismic data can be used to determine seismic velocities from which we can obtain estimates of certain elastic parameters. Examination of equation (18) provides insight on the relationship between the seismic velocities and the elastic parameters of the medium. Horizontally and vertically traveling waves are related to the elastic parameters in the straightforward manner shown in Table 1. In directions between horizontal and vertical, qP and qSV wave speeds depend on A_{11}, A_{33}, A_{44}, and A_{13}; SH wave speeds depend on A_{44} and A_{66}.

Clear resolution of the five elastic parameters at a particular depth will require observation of all three wave types. These waves must have ray paths which have traversed the depth of interest with propagation directions near vertical (for resolution of A_{33} from qP and A_{44} from qSV and SH), near horizontal (for resolution of A_{11} from qP, A_{66} from SH, and A_{44} from qSV), and between vertical and horizontal (for determination of A_{13} from qP and qSV). To procure this range of observations may require novel experiment design, but estimates of some elastic parameters can be made using presently available measurements.

In some cases, estimates of the elastic parameters can be obtained from velocity measurements made on core samples. Using equation (18), horizontal and vertical velocity measurements provide four of the five elastic parameters (Table 1). A measurement of qP or qSV velocity in a direction between horizontal and vertical can be used to determine A_{13} (Jones and Wang, 1981). In most laboratory experiments on core samples, only vertical and horizontal velocity measurements are made, leaving A_{13} completely undetermined.

Anisotropy caused by periodic structures of a scale large compared to a hand specimen, such as bedding or aligned fractures, will not be evident in a core. For a layered medium the effective anisotropic elastic parameters can be calculated

28

using the parameters of the materials composing the layers (Backus, 1962) as done by Levin (1979). Backus's results provide some general constraints for a material composed of isotropic layers: namely, $A_{11} \geq A_{33}$ and $A_{66} \geq A_{44}$. Schoenberg (1983) has expanded on Backus's averaging technique to express the effects of aligned fractures or cracks in an isotropic material in terms of two dimensionless parameters, E_n and E_t. These are, in effect, ratios of the normal and transverse compliance of the crack–filling material to the compliance of the background material. If the anisotropy is due to horizontal cracking of an isotropic material the effective elastic parameters are:

$$A_{11} = \frac{4\mu(\lambda + \mu)}{\lambda + 2\mu} + \frac{\lambda^2}{(\lambda + 2\mu)(1 + E_n)},$$

$$A_{33} = \frac{\lambda + 2\mu}{1 + E_n}, \qquad A_{13} = \frac{\lambda}{1 + E_n}, \tag{23}$$

and

$$A_{44} = \frac{\mu}{1 + E_t}, \qquad A_{66} = \mu$$

where λ and μ are the Lamé parameters of the unfractured material.

Table 1.–Horizontal and vertical
wave speeds in a transversely
isotropic medium

Wave type	Wave speeds	
	Horizontal	Vertical
qP	$\sqrt{A_{11}}$	$\sqrt{A_{33}}$
qSV	$\sqrt{A_{44}}$	$\sqrt{A_{44}}$
SH	$\sqrt{A_{66}}$	$\sqrt{A_{44}}$

VII.   Model Comparisons

Inversion of synthetic travel times from a known structure provides a means of comparing isotropic and transversely isotropic models obtained from travel time analysis. This is necessary for two purposes. First, we need to know the severity of errors introduced if it is assumed that a transversely isotropic structure is isotropic. Second, we must determine what degree of anisotropy might be hidden in existing data.

In the examples discussed here, only a single refraction branch of the travel time curve is used; the inversion is then highly underdetermined and, without additional information or constraints, an isotropic model (with only one parameter) will suffice. My goal is not to define a model, but to determine how a transversely isotropic model will differ from an isotropic one. I then use these models to look for clues in existing seismic data to indicate the presence or absence of transverse isotropy.

Case 1: A Transversely Isotropic Carbonate Model

Milholland et al. (1980) have presented a geoacoustic model for deep sea carbonate sediments based on velocity measurements of DSDP cores from site 289 in the Ontong-Java Plateau. Their model specifies the average compressional and shear velocities at depths of 0, 200, 600 and 1000 meters. Also specified are the density, the ratio of horizontal to vertical wave speeds for qP and SH waves, and the difference in qSV and SH wave speeds in the horizontal plane.

I have used the velocities specified in the Milholland model to determine values for A_{11}, A_{33}, A_{44}, and A_{66} appropriate for a carbonate sedimentary sequence at particular depths. The vertical and horizontal wave speeds are assumed to vary linearly between these depths so that the functional form of the elastic parameters is $A = (az + b)^2$ where z is depth and a and b are constants. Using the results of Section IV, ranges and travel times are calculated for a range of take off angles (ray parameters). These travel times are then used in a tau-sum inversion, as described by Diebold and Stoffa (1981) and shown in Section IV, equation (21), to obtain an isotropic velocity depth model.

Milholland et al.'s measurements provide three of the four elastic parameters required for calculation of travel times and ranges for qP and qSV wave propagation. Equation (22) provides an upper constraint on the value of A_{13}. Because the shape of the wave front (Figure 7) is highly dependent on A_{13} (Dellinger and Muir, personal communication, 1985) it is important to constrain this value well. Bachman (1983) has attempted to determine appropriate values of A_{13} for chalk and limestone; but as he shows, without direct velocity measurements in some direction between horizontal and fill estimates of A_{13} are highly uncertain.

Travel time curves have been computed for three models, listed in Table 2, each with a different set of A_{13} values. All values are well within the allowable range for

31

A_{13} and there is no reason to suspect that any are physically unreasonable. The results of the tau-sum velocity inversions are listed in Table 3 and plotted in Figure 8. Also plotted are the vertical and horizontal qP velocities, essentially $\sqrt{A_{33}}$ and $\sqrt{A_{11}}$, of the starting anisotropic models.

The velocity models obtained with the tau-sum inversions match the travel times exactly. The tau-sum inversion determines the velocity of the ray at its turning point. This gives a correct horizontal velocity, but because of the variation of wave speed with ray parameter in the overlying layers, the layer thickness is incorrectly estimated. In these three models (seen in Figure 8, and apparent when comparing the original anisotropic model in Table 2 to the results of the P wave travel time inversion in Table 3) the overestimate in depth ranges from 3% to 14%. The difference between horizontal and vertical qP wave speed is the same for all models, ranging from 0% at the top to 7.7% at 1000 meters.
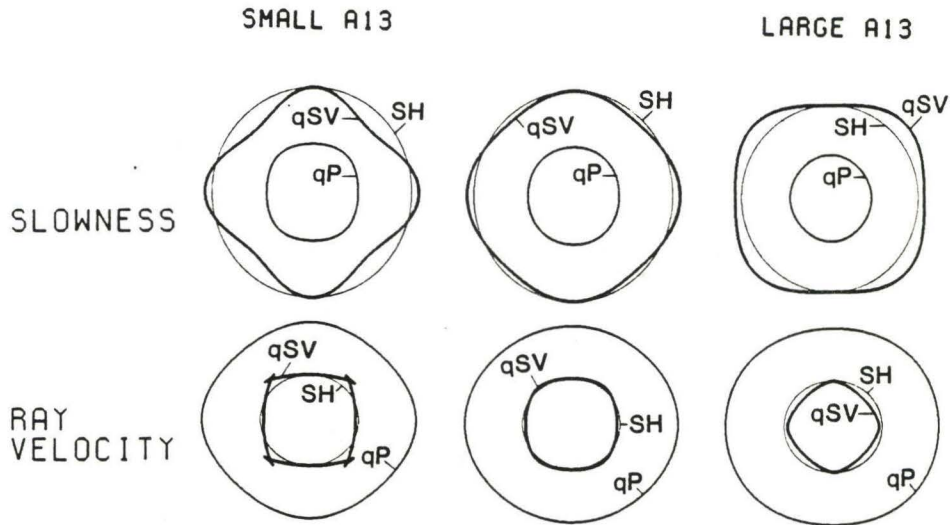
Figure 7: Slowness curves (above) and corresponding ray velocity curves (below) for the three anisotropic carbonate models of Case 1 at 1000 meters depth.
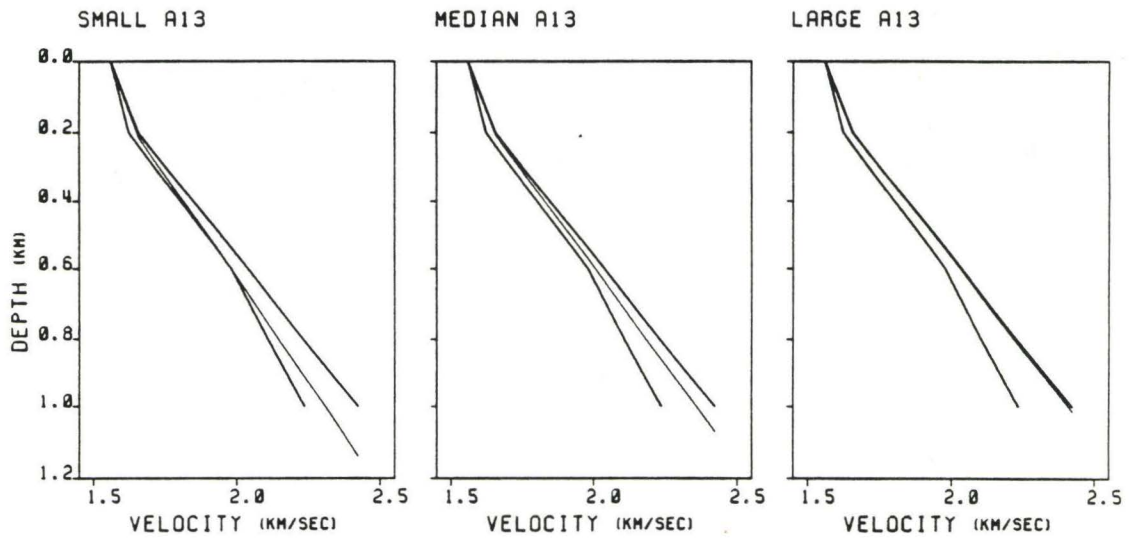
Figure 8: Anisotropic qP velocity depth profiles (heavy lines) with the corresponding isotropic tau–sum P inversion (light line in each figure) for the three carbonate models of Case 1. The two lines of the anisotropic qP profile represent the horizontal (fast) and vertical (slow) qP wave speeds with depth. The actual ray velocity at any depth will fall somewhere between these values depending on the direction of wave propagation at that depth. The isotropic profile is a smoothed plot of the step function obtained with the tau–sum inversion.

33

Table 2.–Elastic parameters for the anisotropic carbonate models of Case 1. The three sets of A_{13} values are shown; the values for A_{11}, A_{33}, and A_{44} are the same in each model.

Depth (km)	$A_{IJ} = C_{IJ}/\rho$ (km/sec)^2			A_{13} for each model		
	A_{11}	A_{33}	A_{44}	Small	Median	Large
0	2.434	2.434	0.004	2.426	2.426	2.426
0.2	2.744	2.636	0.173	2.049	2.223	2.398
0.6	4.158	3.924	0.655	2.034	2.441	2.849
1.0	5.872	5.003	1.075	2.023	2.872	3.721

Table 3.–Depths obtained with isotropic inversions of travel times generated with the models of Table 2. The isotropic P and S velocities at the top and bottom of each layer are equal to the corresponding horizontal qP and qSV wave speeds in the anisotropic model. The isotropic P and S profiles are obtained independently with separate travel time inversions.

	Depths (km)					
	P wave inversion			S wave inversion		
Anisotropic Model	Small A_{13}	Median A_{13}	Large A_{13}	Small A_{13}	Median A_{13}	Large A_{13}
0.200	0.213	0.206	0.200	0.146	0.177	0.228
0.600	0.670	0.636	0.606	0.571	0.626	0.671
1.000	1.140	1.072	1.014	0.944	1.027	1.180

Case 2: Oceanic Layer 2

Case 1 showed that an isotropic model adequately fits refracted P wave travel times from an anisotropic sedimentary structure. The same is true for an anisotropic cystalline crust.

Transverse isotropy in oceanic Layer 2, although not explicitly required by seismic evidence to date, is inferred from other observations. Borehole televiewer records of DSDP borehole 504B indicate a predominant subhorizontal structure throughout the depth of the borehole (Newark et al., 1985). Although presently applicable only to hole 504B, these findings point to strong vertical anisotropy in the upper oceanic crust. Fryer et al. (1987) suggest that this anisotropy will be greatest in young oceanic crust and decrease with age. By finding transversely isotropic models consistent with travel times predicted with existing isotropic crustal models we may delineate the possible extent of this anisotropy.

Bratt and Purdy (1984) have presented a series of detailed P wave velocity profiles for oceanic Layer 2 based on Rivera Ocean Seismic Experiment (ROSE) refraction data obtained along the East Pacific Rise. These profiles were determined using both travel time information and amplitude patterns evident in the data. I have used their model b8 (Bratt and Purdy, 1984, pg. 6119) to compute travel times and ranges for the P-wave refraction branch. I then used an iterative nonlinear inversion to find transversely isotropic models which matched these travel times.

The inversion procedure is based on the ideas presented in Tarantola and Valette (1982) and in Jackson and Matsu'ura (1985). As with all nonlinear inversion schemes, a region of model space in some sense local to a given starting model is searched to better match the given data. In this case, for lack of any more appropriate distribution to use, the data and model parameters are assumed to be Gaussian variables and the data is matched in a least–squares sense.

35

The procedure allows the use of *a priori* information about the model parameters in directing the search in model space. In this case, an *a priori* variance is specified for each parameter of the starting model. The search for a better fitting model is conducted using the information provided by the data and the constraints provided by the *a priori* model variance. Information from the data pertinent to any particular model parameter will reduce the variance of that parameter; thus, this procedure allows one to determine which model parameters can be resolved and precisely what observations are required to resolve each parameter.

The transversely isotropic model is divided into layers. The model parameters are the layer thicknesses and the values of A_{11}, A_{13}, A_{33}, and A_{44} (for qP and qSV propagation) at the top and bottom of each layer. Within a layer the elastic parameters are functions of depth z of the form $A = (az + b)^2$. This produces a linear depth variation in the horizontal and vertical wave speeds within each layer.

Data consisting only of refracted P wave travel times is insufficient to resolve a transversely isotropic model; the problem is highly underdetermined. My goal is to find models with a specified amount of P wave anisotropy which will match the given travel times.

The ray parameter of an arrival provides the inverse of the horizontal velocity of the ray at its turning point. This provides estimates for the value of A_{11}; these are the same values found by the isotropic inversion but occurring at different depths. Values for A_{33} are then set to give the desired horizontal to vertical qP velocity ratio. Because Bratt and Purdy (1984) provided no shear velocity model (no converted arrivals were observed), values for A_{44} were determined by assuming a value of Poisson's ratio for the horizontal qP and qSV wave speeds judged appropriate for the upper oceanic crust. The horizontal Poisson's ratio for the models was .33 at the surface and decreased smoothly to a constant value of .28 from the depth at which the horizontal qP velocity was 5.5 km./sec.

36

The *a priori* variance for the model parameters A_{11}, A_{33}, and A_{44} was set to zero at all depths, thereby holding these values constant in the search through model space. The *a priori* variance for A_{13} and the layer thicknesses was set to a very high number, greater than 1000 times the initial estimates, indicating no prior knowledge of these parameters.

With the constraints on A_{11}, A_{33}, and A_{44} the problem is overdetermined and the values of A_{13} and the layer thicknesses are well resolved by the data. For each example shown the fit to the synthetic data had a standard deviation of less than 0.01 seconds.

Models with 10%, 25%, and 40% P wave anisotropy were found, with the anisotropy decreasing to zero at the base of layer 2. The horizontal and vertical qP wave speeds are plotted in Figure 9 overlain with the isotropic velocity model used to generate the travel times. The depth to the base of layer 2 predicted by each model varies from 1.9 km. for the isotropic case to 1.4 km. for the model with 40% anisotropy (Table 4).

The constraints placed on the above models are rather arbitrary. Estimates of appropriate values for the elastic parameters of a transversely isotropic oceanic crust are essentially guesses. The values of A_{11} and A_{44} are constrained by the horizontal velocities determined from refraction lines. Unfortunately, resolution for the shallow crust is often poor and shear wave data is generally lacking. To resolve transverse isotropy with travel time information requires both P and SV (qP and qSV) data with narrow to wide angle coverage so that both reflected rays and rays turning throughout the depth section are sampled. SH arrivals will further constrain estimates of A_{44} and will provide information on A_{66}.

Table 4

Models of oceanic Layer 2A for Case 2.

Isotropic Model				
Depth (km)	A_{11} $(km/sec)^2$	A_{33} $(km/sec)^2$	A_{44} $(km/sec)^2$	A_{13} $(km/sec)^2$
0.000	4.410	4.410	1.119	2.172
0.700	30.250	30.205	9.243	11.764
1.100	30.250	30.250	9.243	11.764
1.900	47.610	47.610	14.547	18.516
5.500	50.410	50.410	15.403	19.604
6.500	64.000	64.000	19.555	24.890

10% Anisotropy				
Depth (km)	A_{11} $(km/sec)^2$	A_{33} $(km/sec)^2$	A_{44} $(km/sec)^2$	A_{13} $(km/sec)^2$
0.000	4.410	3.572	1.119	1.747
0.638	30.250	24.503	9.243	10.000
1.005	30.250	24.503	9.243	10.000
1.771	47.610	47.610	14.547	18.516
5.368	50.410	50.410	15.403	19.604
6.359	64.000	64.000	19.555	24.890

25% Anisotropy				
Depth (km)	A_{11} $(km/sec)^2$	A_{33} $(km/sec)^2$	A_{44} $(km/sec)^2$	A_{13} $(km/sec)^2$
0.000	4.410	2.481	1.119	1.120
0.552	30.250	17.016	9.243	8.000
0.885	30.250	17.016	9.243	8.000
1.590	47.610	47.610	14.547	18.516
5.183	50.410	50.410	15.403	19.604
6.150	64.000	64.000	19.555	24.890

40% Anisotropy				
Depth (km)	A_{11} $(km/sec)^2$	A_{33} $(km/sec)^2$	A_{44} $(km/sec)^2$	A_{13} $(km/sec)^2$
0.000	4.410	1.588	1.119	0.411
0.470	30.250	10.890	9.243	6.000
0.791	30.250	10.890	9.243	6.000
1.429	47.610	47.610	14.547	18.516
5.015	50.410	50.410	15.403	19.604
6.029	64.000	64.000	19.555	24.890

Discussion

The previous examples show that the presence of transverse isotropy can result in significant inaccuracy in isotropic estimates of layer thicknesses and elastic properties. Transverse isotropy has been suggested in several cases to explain apparent discrepancies in seismic data. In the North Sea basin seismically determined depths to major reflectors are systematically greater than well log depths. Banik (1986) shows that this disagreement is explained by the presence of transversely isotropic shales in the section. Davis and Clowes (1986) suggest that the anomalously high (horizontal) sediment velocities seen in bedded turbidite sediments of the Winona Basin are indicative of transverse isotropy. Fryer (1986) has invoked a decrease of transverse isotropy with age in the upper oceanic crust to explain the apparent thinning of layer 2A. Analysis of synthetic travel time data can suggest ways of looking at existing data for indications of transverse isotropy.

For refraction data, shear wave arrivals are essential. Fryer and Miller (1986) have shown that independent isotropic inversions of P and SV travel times from a transversely isotropic structure result in mismatches in layer thickness estimates and erroneous estimates of Poisson's ratio. Tau-sum inversions of refracted qSV arrivals for the three carbonate models previously presented in case 1 give the depths (Table 3) shown in Figure 10. For the isotropic inversions, the shear velocity models show an even greater variation with A_{13} than the compressional velocity models show. More important for this analysis is a comparison of the P and S velocity models obtained in an individual case. For models with large and small values of A_{13}, the differences between the P and S estimates of layer thicknesses (Table 3) are within the resolution obtainable using marine data.

Travel times for the carbonate models were computed ignoring the ocean layer. For actual data, with a source at the ocean surface, the shallowly turning arrivals

39

can be difficult to distinguish due to interference from the direct water wave (for an OBS) or from the bottom reflection (in sonobuoy records); good model resolution is then hard to obtain. For an ocean source the shallow shear wave structure will be inaccessible to refraction analysis. Low shear wave speeds in sediments preclude turning rays above depths where shear wave speeds are less than the compressional wave speed in water. Detection of anisotropy in marine sediments may require greater resolution than is attainable with a surface source.

Marine records often show arrivals interpreted as converted shear waves with ray paths which turn in the igneous basement. These arrivals have been used for determination of a shear velocity structure for the oceanic crust (Spudich and Orcutt, 1980a,b; Shearer and Orcutt, 1986; Duennebier et al., 1985). Tau-sum inversions of shear arrivals for the three anisotropic models found in case 2 give the S velocity models shown in Figure 11 and in Table 5. Turning rays to the Moho transition have been included because the anisotropy near the surface also affects isotropic estimates of layer thicknesses for the deeper layers. Discrepancies in the isotropic P and S models occur in each case; the differences in layer depth estimates between the two increase with increasing P wave anisotropy. The differences apparent in Figure 12 and Table 5 are withen the resolution of good seismic data and should be expected if Layer 2 is transversely isotropic. Indeed, such an occurrence is noted by Shearer and Orcutt (1986) for data from the Ngendei refraction experiment.
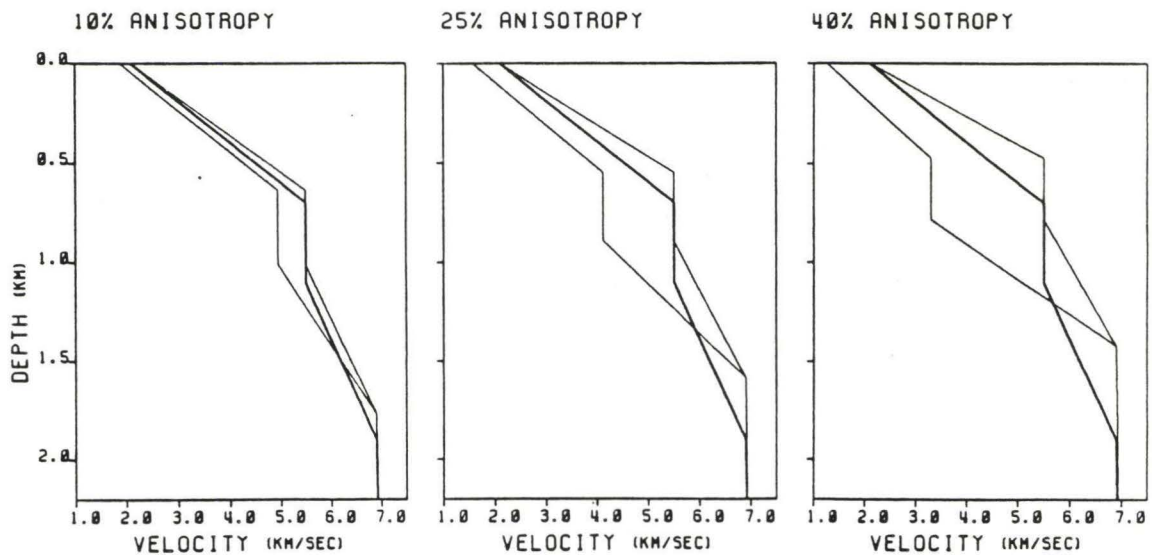
Figure 9: The isotropic P velocity depth profile (heavy line in each figure) for oceanic Layer 2 from Bratt and Purdy (1984) and the three anisotropic qP profiles (light lines) obtained from travel time inversion in Case 2. The two lines in each anisotropic profile represent the horizontal (fast) and vertical (slow) qP wave speeds.

Table 5.–Layer depths obtained in the isotropic inversion of travel times from the anisotropic models of Table 4. The P wave inversion is the same for all models and matches the original isotropic model of Bratt and Purdy used for Case 2.

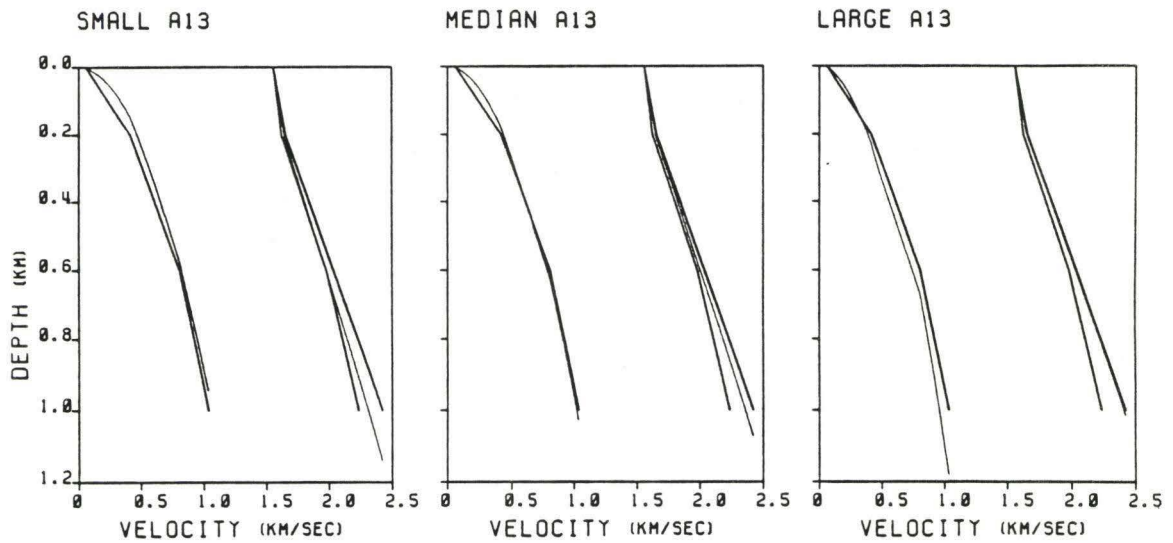| Depths (km)			
P wave inversion	S wave inversion		
	10%	25%	40%
0.700	0.659	0.630	0.623
1.100	1.087	1.230	1.473
1.900	1.823	1.758	1.728
5.500	5.205	5.157	5.037
6.500	6.379	6.212	6.095

41

SMALL A13   MEDIAN A13   LARGE A13

Figure 10: Both the qP and qSV velocity depth profiles of the carbonate models of Case 1 are shown (heavy lines) with the smoothed isotropic P and S profiles (light lines) found with a tau–sum inversion. The isotropic P and S profiles are obtained independently; note that for each of the three models, the layer depth estimates of the isotropic P and S profiles do not match. The velocity profiles of the anisotropic models represent horizontal and vertical wave speeds with depth. For the qP wave the horizontal wave speed is faster than the vertical; for the qSV wave the horizontal and vertical wave speeds are equal.
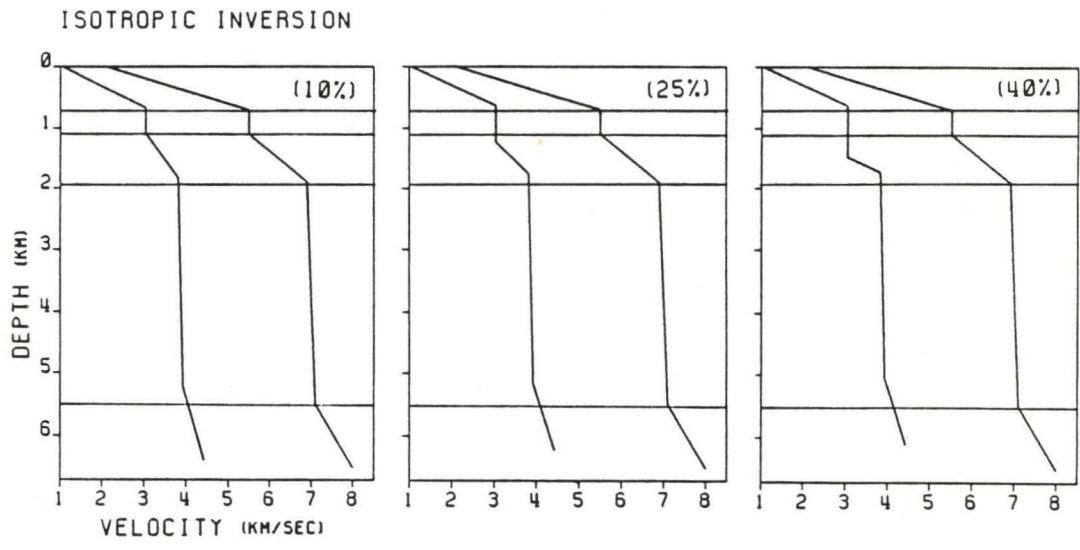
ISOTROPIC INVERSION

Figure 11: Smoothed isotropic P and S velocity depth profiles obtained with tau–sum inversion of travel times from the anisotropic models of oceanic Layer 2 found in Case 2. The horizontal lines indicate depths for layers 2a, 2b, 2c, and 3 in the original Bratt and Purdy (1984) P profile, the travel times of which were used to constrain the anisotropic models. The anisotropic models are shown in Figure 9.

43

VIII.   Apparent Variations in Poisson's Ratio

Because transverse isotropy produces discrepancies in separate inversions of P and SV refraction data, variations occur in the apparent value of Poisson's ratio calculated from the isotropic velocity depth functions. The effect of transverse isotropy on isotropic estimates of Poisson's ratio is highly variable and is dependent upon the nature of the anisotropy, the geometry of the experiment, and the type of travel time inversion used. Unreasonable estimates of Poisson's ratio are diagnostic of transverse isotropy (Fryer and Miller, 1986). The following example illustrates the consequences transverse isotropy may have for estimates of Poisson's ratio for oceanic Layer 2.

I used the P wave model presented by Shearer and Orcutt (1986, pg. 976) for NNE azimuth Ngendei refraction data to generate a travel time curve for the P wave refraction branch. A linear velocity variation was assumed between the depths at which the velocity was specified. As in the previous section, a model with transverse isotropy was found to match the travel times. Again, A_{11} was set to match the (horizontal) P velocities determined from the refraction data and A_{33} was set to produce the desired difference between the vertical and the horizontal qP wave speeds. A_{44} was determined by choosing a Poisson's ratio for the horizontal wave speeds. For this example it was assumed that the anisotropy is caused by a system of horizontally aligned fractures. If a Poisson's ratio for the unfractured isotropic material is assumed, A_{13} can be constrained by the parameter E_n from equation (23). For an isotropic medium:

$$A_{11} = A_{33},$$

$$A_{13} = A_{11} - 2A_{44},$$

and

$$A_{44} = \frac{A_{11}(1 - 2\sigma)}{2 - 2\sigma}$$

where σ is Poisson's ratio. These relations, together with the effective transversely isotropic values of A_{11} and A_{33} and equation (23), determine the effective value of A_{13}. The layer thicknesses are then the only free variables in the inversion. Each anisotropic model found with the inversion fit the synthetic data with a standard deviation of less than 0.03 seconds.

Several anisotropic models were found, each with a different variation of the horizontal Poisson's ratio with depth. A tau-sum inversion of the shear wave travel times was used to find an isotropic S velocity depth function for each model. The isotropic P wave model (Shearer and Orcutt, 1986) and the S wave model are used to calculate the apparent variation of Poisson's ratio with depth (Figures 12–16).

The variation of A_{44} with depth in these models has a profound effect on the computed value of Poisson's ratio in the isotropic inversions. Dips in the apparent value of Poisson's ratio in the upper oceanic crust, such as seen by Shearer and Orcutt (1986), Spudich and Orcutt (1980b), and in Figure 13, can result from an isotropic parameterization of a transversely isotropic structure.
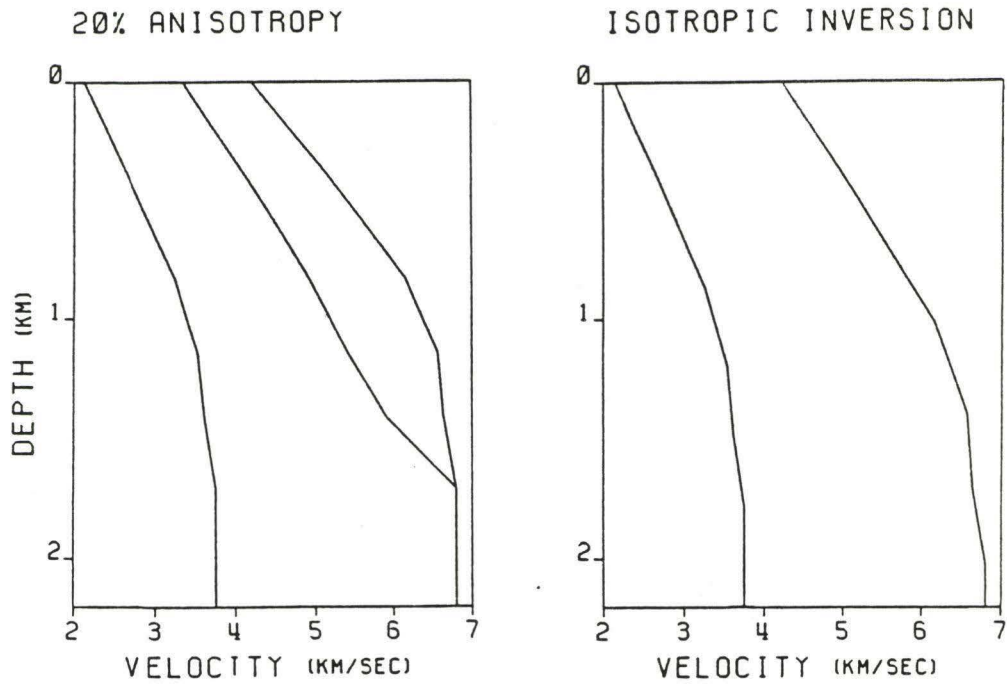
Figure 12: The anisotropic qP and qSV velocity depth profiles (left figure) have travel time curves which produce the isotropic profiles shown on the right. These isotropic profiles match closely those obtained by Shearer and Orcutt (1986) for NNE azimuth Ngendei refraction data. Note the mismatch in the depth obtained for Layer 2 in the P and S profiles on the right, similar to the mismatch seen by Shearer and Orcutt. Such differences in isotropic P and S profiles can be caused by an incorrect isotropic parameterization of a transversely isotropic oceanic crust.
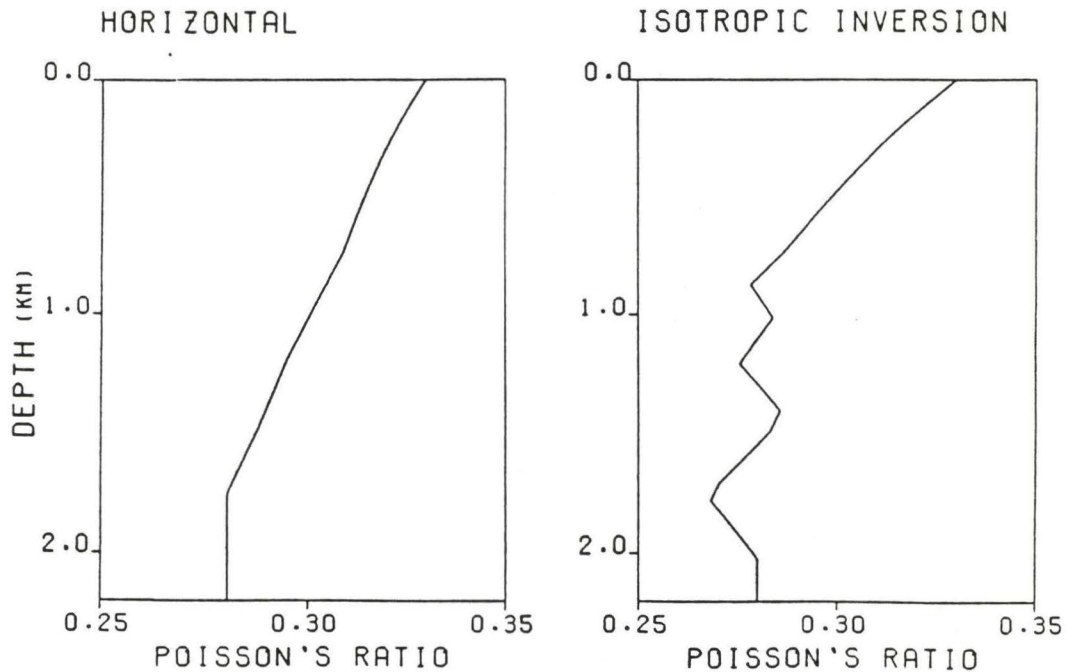
Figure 13: Plots of Poisson's ratio with depth for the velocity profiles of Figure 12. The left figure shows Poisson's ratio calculated using the horizontal qP and qSV wave speeds of the anisotropic model; Poisson's ratio is .33 at the surface and varies to a constant value of .28 from 1.71 km. depth. The right figure shows Poisson's ratio calculated using the P and S wave speeds of the isotropic inversion. Note that Poisson's ratio is consistently underestimated using the isotropic profiles. The jumps in Poisson's ratio with depth seen for the isotropic model (right figure) are due to the differences in layer depths found in the separate P and S inversions. The sharp corners are an artifact of the type of model used; velocities are assumed to vary linearly with depth with discontinuities in the rate of change (i.e. discontinuities in dv/dz). A corner in the Poisson's ratio profile occurs at the depths where dv/dz is discontinuous. A smoother velocity depth profile will produce a smoother Poisson's ratio profile, but the jumps will still occur. Note the sudden decrease seen near 1.7 km. depth, similar to that seen by Shearer and Orcutt (1986) and by Spudich and Orcutt (1985).
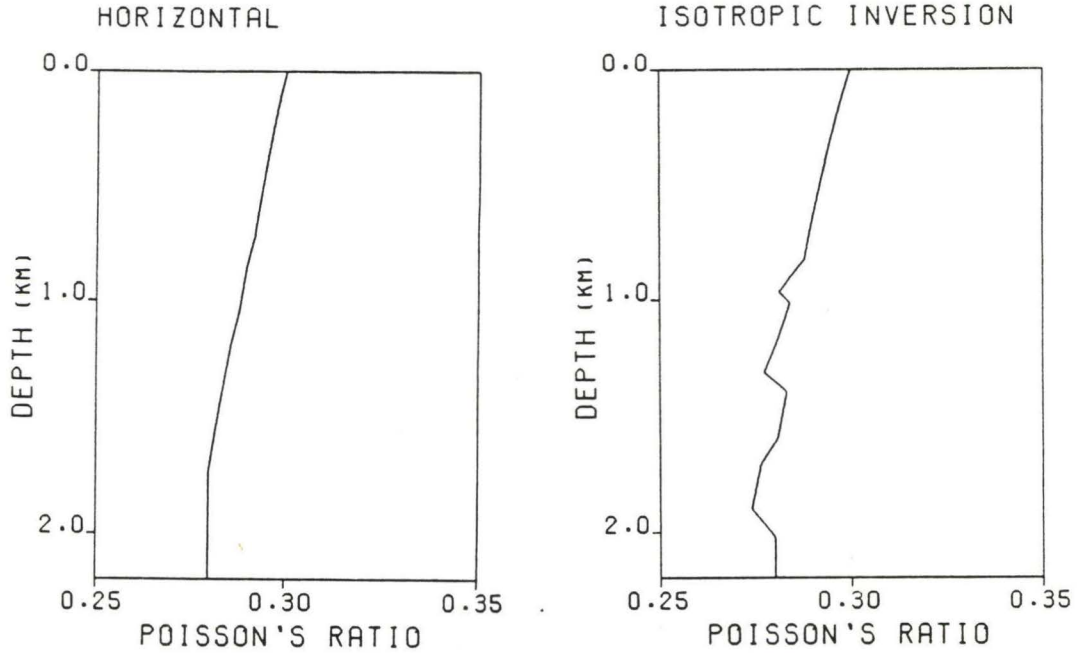
Figure 14: Plots of Poisson's ratio with depth for models with higher qSV (and S) wave speeds than the models of Figure 12. The left figure shows the Poisson's ratio profile calculated using the horizontal qP and qSV wave speeds of an anisotropic model similar to that shown in Figure 12, except that the qSV wave speeds are slightly higher in the upper crust. In this case, Poisson's ratio varies from a value of .30 at the surface to a constant value of .28 from 1.71 km. depth. The figure on the right shows Poisson's ratio calculated using the isotropic P and S velocity depth profiles obtained from inversion of travel times from the anisotropic model. As in Figure 13, Poisson's ratio is consistently underestimated using the isotropic inversion.
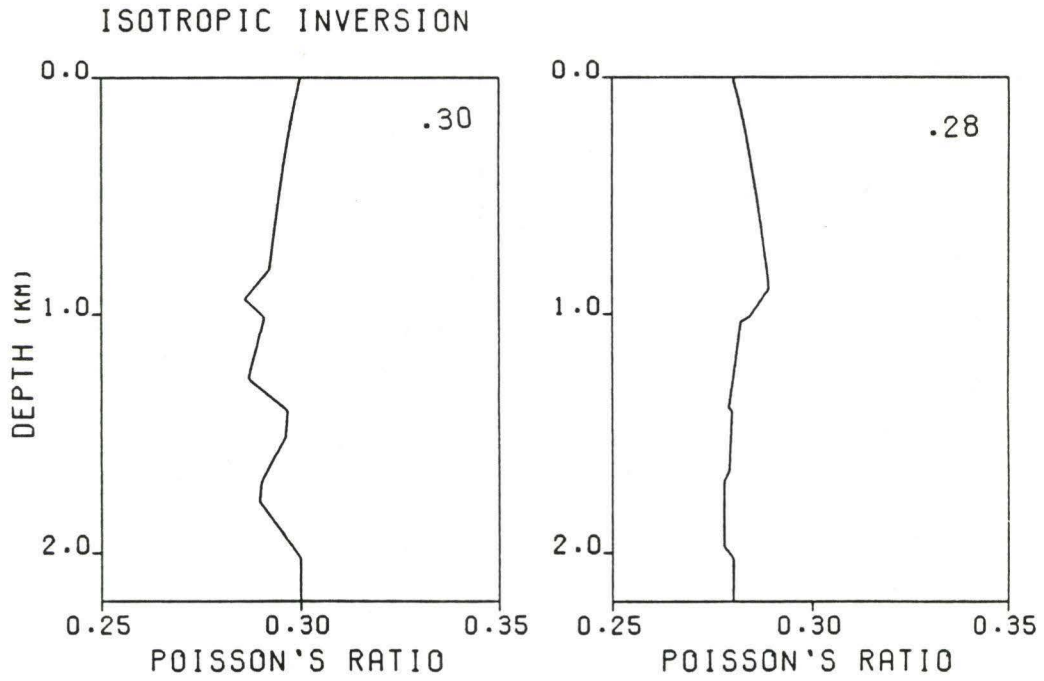
48

Figure 15: Plots of Poisson's ratio with depth found using isotropic P and S velocities obtained from inversion of travel times of anisotropic models for which Poisson's ratio was constant with depth. The anisotropic models were similar to the one shown in Figure 12 with qSV wave speeds adjusted to give constant values of Poisson's ratio at all depths. The plot on the left was calculated using isotropic P and S velocities found from inversion of travel times from an anisotropic model for which Poisson's ratio was .30. Here Poisson's ratio is consistently underestimated with sudden jumps at particular depths. The plot on the right was calculated using isotropic P and S velocities found from inversion of travel times from an anisotropic model for which Poisson's ratio was .28. Here Poisson's ratio is *overestimated* at shallow depths. The value choosen for A_{44} in the anisotropic models, which determines the horizontal and vertical qSV wave speed, has a significant effect on the isotropic inversions obtained and on the profile of Poisson's ratio found using those inversions.
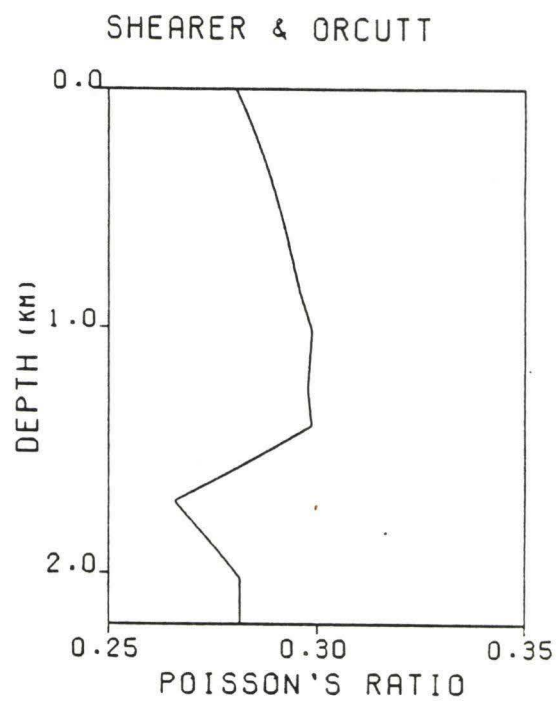
49

SHEARER & ORCUTT

Figure 16: Plot of Poisson's ratio with depth for the isotropic model obtained by Shearer and Orcutt (1986) for NNE azimuth Ngendi refraction data.

IX. Conclusions

Relaxing the constraint of isotropy in the interpretation of seismic data can result in substantial changes in the models obtained. It also results in greater indeterminacy for these models. For example, one suite of P wave refraction data for oceanic Layer 2 is fit equally well by either an isotropic layer 1.9 kilometers thick or by a transversely isotropic layer 1.4 kilometers thick (Table 4). Attributes of existing isotropic models which suggest transverse isotropy, such as steep velocity gradients and dips in Poisson's ratio, bring these models into question. Removal of the indeterminacy in these models requires additional information. The simple analysis presented here suggests which observations are needed:

- Observation of all three wave types.

- Narrow to wide angle coverage.

- Detailed resolution of the shallow crust.

Resolution of symmetries with order less than that of transverse isotropy will require source–receiver geometries spanning two or even three dimensions.

Travel time inversion is computationally very fast compared to waveform analysis. Eventually, confidence in modeling the oceanic crust will require a look at waveforms. The possibility of transverse isotropy along with the observation of azimuthal anisotropy indicates that lower symmetry systems (e.g. orthorhombic, monoclinic) must be examined. This work serves mainly as a warning to those who place too much confidence in inversions which tacitly assume isotropy.

References

Aki, K. & Richards, P. G., 1980. *Quantitative Seismology, Theory and Methods, Vol. 1*, W. H. Freeman & Company, San Francisco.

Auld, B. A., 1973. *Acoustic Fields and Waves in Solids, Vol. 2*, John Wiley & Sons, New York.

Bachman, R. T., 1979. Acoustic anisotropy in marine sediments and sedimentary rocks, *J. geophys. Res.*, **84**, 7661–7663.

Bachman, R. T., 1983. Elastic anisotropy in marine sedimentary rocks, *J. geophys. Res.*, **88**, 539–545.

Backus, B. E., 1962. Long-wave elastic anisotropy produced by horizontal layering, *J. geophys. Res.*, **67**, 4427–4440.

Bamford, D. & Crampin, S., 1977. Seismic anisotropy–the state of the art, *Geophys. J. R. astr. Soc.*, **49**, 1–8.

Banik, N. C., 1984. Velocity anisotropy of shales and depth estimation in the North Sea basin, *Geophysics*, **49**, 1411–1419.

Bratt, S. R. & Purdy, G. M., 1984. Structure and variability of oceanic crust on the flanks of the East Pacific Rise between 11° and 13°N., *J. geophys. Res.*, **89**, 6111–6125.

Byun, B. S., 1984. Seismic parameters for transversely isotropic media, *Geophysics*, **49**, 1908–1914.

Červený, V., Molotkov, I. A., & Pšenčí, I., 1977. *Ray Method in Seismology*, Univerzita Karlova, Praha.

Crampin, S., 1987. A consistent notation for seismic anisotropy, *Geophysics*, submitted.

Crampin, S., Chesnokov, E. M., & Hipkin, R. G., 1984. Seismic anisotropy-the state of the art: II, *Geophys. J. R. astr. Soc.*, **76**, 1-16.

Crampin, S. & Radovich, B., 1982. Interpretation of synthetic common–depth–point gathers for a single anisotropic layer, *Geophysics*, **47**, 323–335.

Courant, R. & Hilbert, D., 1962. *Methods of Mathematical Physics, Vol. 2*, John Wiley & Sons, New York.

Davis, E. E. & Clowes, R. M., 1986. High velocities and seismic anisotropy in Pleistocene turbidites off Western Canada, *Geophys. J. R. astr. Soc.*, **84**, 381–399.

Diebold, J. B. & Stoffa, P. L., 1981. The traveltime equation, tau–p mapping, and inversion of common midpoint data, *Geophysics*, **46**, 238–254.

Dorman, L. M. & Jacobson, R. S., 1981. Linear inversion of body wave data–Part 1: Velocity structure from traveltimes and ranges, *Geophysics*, **46**, 138–151.

Duennebier, F. K., Lienert, B., Cessaro, R., Anderson, P., & Mallick, S., 1987. Controlled–source seismic experiment at hole 581–C, *Initial Reports of the Deep Sea Drilling Project*, **89**, 105–125.

Fryer, G., 1986. Transverse isotropy and the thickness of layer 2A, *EOS*, **67**, 1083.

Fryer, G. & Miller, D., 1986. Effects and consequences of transverse isotropy in the seafloor, *Ocean Seismo-Acoustics*, Tuncay & Berkson, editors, Plenum Publishing Corp., New York.

Fryer, G., Miller, D., & Berge, P., 1987. Transverse isotropy and age–dependent structure of the upper oceanic crust, *International Union of Geodesy and Geophysics, XIX General Assembly, Abstracts*, **1**, 84.

Hamilton, E. L., 1979. Sound velocity gradients in marine sediments, *J. acoust. Soc. Am.*, **65**, 909–922.

Jackson, D. & Matsu'ura, M., 1985. A Bayesian approach to nonlinear inversion, *J. geophys. Res.*, **90**, 581–591.

Jones, L. & Wang, H., 1981. Ultrasonic velocities in Cretaceous shales from the Williston basin, *Geophysics*, **46**, 288–297.

Kraut, E. A., 1963. Advances in the theory of anisotropic elastic wave propagation, *Rev. of Geophys.*, **1**, 401–448.

Milholland, P., Manghnani, M., Schlanger, S., & Sutton, G., 1980. Geoacoustic modeling of deep–sea carbonate sediments, *J. acoust. Soc. Am.*, **68**, 1351–1360.

Levin, F. K., 1979. Seismic velocities in transversely isotropic media, *Geophysics*, **44**, 918–936.

Newmark, R.L., Anderson, N., Moos, D., & Zaback, M. D., 1985. Sonic and ultrasonic logging of hole 504b and its implications for the structure, porosity, and stress regime of the upper 1 km of the oceanic crust, *Initial Reports of the Deep Sea Drilling Project*, **83**, 479–510.

Schoenberg, M., 1983. Reflection of elastic waves from periodically stratified media with interfacial slip, *Geophysical Prospecting*, **31**, 265–292.

Shearer, P. M. & Orcutt, J. A., 1986. Compressional and shear wave anisotropy in the oceanic lithosphere–the Ngendei seismic refraction experiment, *Geophys. J. R. astr. Soc.*, **87**, 967–1003.

Spudich, P. & Orcutt, J. A., 1980a. Petrology and porosity of an oceanic crustal site: results from wave form modeling of seismic refraction data, *J. geophys. Res.*, **85**, 1409–1433.

Spudich, P. & Orcutt, J. A., 1980b. A new look at the seismic velocity structure of the oceanic crust, *Rev. of Geophys. and Space Phys.*, **18**, 627–645.

Stephen, R. A., 1985. Seismic anisotropy in the upper oceanic crust, *J. geophys. Res.*, **90**, 11383–11396.

Tarantola, A. & Valette, B., 1982. Generalized nonlinear inverse problems solved using the least squares criterion, *Rev. of Geophys. and Space Phys.*, **20**, 219–232.